In: Monomers, Oligomers, Polymers, Composites… ISBN: 978-1-60456-877-6
Editors: R. A. Pethrick, G.E. Zaikov et al.

Chapter 16

"GLASSCRETE" CONTAINING POLYMER AGGREGATE AND POLYAMIDE FIBERS

A. Sadrmomtazi and A. K. Haghi*
University of Guilan; P.O. Box: 3756; Rasht, Iran

ABSTRACT

In this chapter the behavior of lightweight EPS glasscrete containing polymeric fibers are studied. The results are compared together and with the results observed by other authors. The comparison revealed the superiority of this new composite in improving the compressive and tensile strength. The results are indicative of strong potentials for application of waste polymeric fibers for the reinforcement of lightweight EPS glasscrete products.

INTRODUCTION

Concrete is the most widely used construction material in the world. Its low cost, ease of application and compressive strength are the principle reasons for its universal acceptance. However it has few shortcomings most of which are attributable to the Portland cement binder. Shortcomings include poor tensile strength, high porosity freeze thaw deterioration, and destruction by corrosive chemicals, etc. [1]

The development of new composite materials possessing increased strength and durability when compared with conventional types is a major requirement of applications in repairs and in the improvement of infrastructure materials used in the civil construction industry. Polymer concrete (PC) is an example of a relatively new material with such high performance [2].

The demand for lightweight concrete in many applications of modern construction is increasing, owing to the advantage that lower density results in a significant benefit in terms

* Corresponding author e-mail: Haghi@Guilan.ac.ir

of load-bearing elements of smaller cross sections and a corresponding reduction in the size of the foundation [3].

Lightweight aggregate concrete, popular through the ages, was reported to have a comparable or some times better durability even in severe exposure conditions.

Lightweight aggregates are broadly classified in to two types: natural (pumice, diatomite, volcanic cinders, etc.) and artificial (perlite, expanded shale, clay, slate, sintered PFA, etc.). Expanded polystyrene (EPS) beads are a type of artificial ultra-lightweight, non-absorbent aggregate [4, 5]. It can be used to produce low-density concretes required for building applications like cladding panels, curtain walls, composite flooring systems, and load-bearing concrete blocks [6, 7].

Expanded polystyrene (EPS) concrete is a lightweight concrete with good energy-absorbing characteristics, consisting a discrete air voids in a polymer matrix. However, polystyrene beads are extremely light, with a density of only 12 to 20, which can easily cause segregation in mixing. Hence some chemical treatment of surface on this hydrophobic material is needed. Other investigators also reported that EPS tends to float and can result in a poor mix distribution and segregation, necessitating the use of admixtures [8, 9].

Our main aim is to contribute to the understanding of the behaviour of EPS Glasscrete reinforced with polyamide fibers. The quantity of fibers used is small, typically 1 to 5 per cent by volume.

BACKGROUND

In general, waste glass produced can be sorted out as:

- building/automobile windows and doors;
- glassware and bottles;
- television tubes and light bulbs;
- others such as mirror and clock covers.

Among them, the first two are the major sources. Several domestic glass manufacturers have attempted to recycle the glass waste.

Waste recycling has become increasingly important for western society over the past few years. The European desire to increase recycling of glass, particularly that of glass bottles, has led to a large collect system in containers and a target of 75% of the collected glass (2.2 million tons) recycled by the year 2005 in France . Nevertheless, there will still be 5% of collected glass(0.1 to 0.15 million tons) that is not recycled and must be disposed of, as glass can only be melted down after the removal of non-ferrous metals and other contaminants, which are mixed with the smallest glass fragments . For the long period of disposal, it is predicted that the waste glass will corrode very slowly by contact with groundwater, and certain quantities of radionuclides will be released from the glass. Therefore, the waste glass corrosion and associated radionuclide release for the long-term are one of the most important phenomena to be evaluated for safety assessment of the disposal system .

Glass is a thermodynamically metastable, highly viscous liquid phase. When glass is placed in aqueous environments, various reactions, such as ion exchange, hydrolysis and

transformation to more stable phases, occur simultaneously, and the effects of these reactions are generally referred to as “corrosion”. However, the glass corrosion allows the release of radionuclides from glass, and the glass corrosion and associated radionuclide release for the long- term must be evaluated sufficiently .

Concrete, the composite material consisting of aggregate held together by a hydraulic cementing agent, has been known to ancient civilizations. In spite of its worldwide popularity, the proliferation of concrete has been a mixed blessing. If mixed or placed improperly or maintained inadequately, concrete structures can deteriorate prematurely and thereby contribute to the problems referred to generally as our “crumbling infrastructure”. Also the indiscriminate use of concrete without concern for esthetic appearance has led to the partially deserved reputation of concrete as being ugly. More significantly, the increased worldwide concern about environmental issues and the need to change our way of life for the sake of sustainable development has led to the identification of the concrete industry as a major user and abuser of natural resources and energy and as an important contributor to the release of greenhouse gases. These issues pose formidable challenges for the concrete industry for years to come. The construction community as well as the public at large will demand increased emphasis on environmentally friendly high-performance building materials at affordable cost. This implies not only excellent mechanical properties but durability as well. Fortunately, concrete materials science has emerged as a tool well suited to face these issues .

The introduction and development of advanced composite material opened the door to new and innovative application in civil and structural engineering. Key points of this investigation are:

1. To convert glass and carpet waste into useful product.
2. To consume glass and carpet wastes which would otherwise gone to landfill.
3. Protection of Environment from being heavily contaminated

In developing concrete products with crushed waste glass aggregate, the economics is controlled by the price the product can fetch on the open market. Commodity products, by definition, are characterized by low values, which exert strong pressures on the production and manufacturing technology. The value added by the glass is marginal to nonexistent in those cases. But by utilizing the special properties of glass, chemical, physical, or esthetic, novel products can be developed, for which the prices fetched in the open market are much less exposed to competitive pressures.

What makes glass such a special ingredient for concrete becomes apparent by summarizing its special properties:

- Because it has basically zero water absorption, it is one of the most durable materials known to man. With the current emphasis on durability of high-performance concrete, it is only natural to rely on extremely durable ingredients.
- The excellent hardness of glass gives the concrete an abrasion resistance that can be reached only with few natural stone aggregates.
- For a number of reasons, glass aggregate improves the flow properties of fresh concrete so that very high strengths can be obtained even without the use of superplasticizers .

- The esthetic potential of color-sorted post-consumer glass, not to mention specialty glass, has barely been explored at all and offers numerous novel applications for design professionals.
- Very finely ground glass has pozzolanic properties and therefore can serve both as partial cement replacement and filler.

Waste glass can be used as partial replacement of coarse aggregate, fine aggregate, cementitious materials or ultra fine filler in concrete, depending on its chemical composition and particle size. Previous efforts have been made shown that replacement of glass as a part of coarse aggregate was not satisfactory because of chemical reaction between the alkali in the cement and the silica in the glass. This strongly expansive alkali-silica reaction (ASR) creates a gel, which swells in the presence of moisture, causes cracking and unacceptable damage of the concrete. Recent studies have shown that if the waste glass finely ground, could be used in mortars and concrete as a very fine addition without introducing problems concerning ASR. In fact, a general conclusion of literatures shows that if the waste glass is finely ground under 75μm, ASR does not occur and mortar durability is guaranteed because of its pozzolanic properties. Also on a market price basis, it would be much more profitable to use the glass in powder form as cement replacement to make a value added composite cement.

EXPERIMENTAL PROCEDURE

Materials

Ordinary Portland cement (OPC) was used. The main chemical composition of (OPC) used in this study are listed in table 1.

Table 7. Chemical and physical compositions of ordinary Portland cement

Sio_2	20.40%
Al_2o_3	6.12%
Fe_2O_3	3.051%
CaO	63.16%
MgO	2.32%
SO_3	2.40%
Specific gravity	3.13

Two types of commercially available spherical EPS beads were used (table 2). As indicated in table 2, the grading of EPS shows that type A has mostly 6.0-mm-size beads and type B has mostly 3.0-mm-size beads.

Table 8. EPS beads characteristics

Type	Size (mm)	Bulk density (kg/m^3)	Specific gravity
A	6	16	0.014
B	3	20	0.029

The physical properties of PA 66 used in this study are summarized in table 3.

Table 9. Physical properties of Polyamide fibers used

Specific gravity	1.16
Tensile strength	965 MPa
Elastic modulus	5.17 GPa
Ultimate elongation	20%

Glasscrete Preparation

The cement replacement by the ground waste glass was 10%, 20%, 30% and 40% by total weight.

The composite cement paste containing ground waste glass were compared to the cement having the same percent replacement by silica fume and rice husk ash as well as to the control specimen without any mineral additives. The five batches were defined as follows:

- Ordinary Portland cement paste: no mineral additives
- Waste glass type I: 10%, 20%, 30% and 40% by weight of the Portland cement replaced by waste glass type I
- Waste glass type II: 10%, 20%, 30% and 40% by weight of the Portland cement replaced by waste glass type II
- Silica fume: 10%, 20%, 30% and 40% by weight of the Portland cement replaced by waste silica fume
- Rice husk ash: 10%, 20%, 30% and 40% by weight of the Portland cement replaced by husk rice ash.

Specimen Preparation

A number of standard test specimens of different sizes were selected for investigating the various parameters. For studying the compressive strengths at 3, 7, and 28 days and also for investigating the absorption tests cubes of 100 mm size were used. Meanwhile, the split tensile strength test was conducted on 100 mm diameter × 200 mm cylinders at 28 days.

Lightweight EPS glasscrete were made with PA and without PA reinforcement. Initially, the EPS beads were wetted with 25% of the mixing water and superplasticizer before adding the remaining materials. It is expected that by addition of EPS in place of normal aggregate the weight of glasscrete can be reduced significantly and the interaction of Polyamide 66 fibers with EPS concrete can improve the strength. In this study, the estimated component additions were measured by volume in order to simplify mixing process. The non-absorbent, hydrophobic and closed cellular aggregates (expanded polystyrene beads) were mixed in a planetary mixer in compliance with the recommendation of ASTM C 305. To obtain a very uniform and flowing mixture, the mixing operation was continued on a regular bias. The molds are then filled with fresh EPS concrete and then with PA reinforced EPS concrete. Afterward, the mixture is firmly compacted by hand.

Based on ASTM C 143-98 we measured the slump values of the fresh concrete. Afterward, the compressive strength test was carried out in a testing machine with capacity of 2000 KN. The loading rate used during this test was 2.5 KN/s. According to ASTM C 496-89 we conducted the split tensile strength test on cylinders at 28 days. The absorption test was then carried out as per ASTM C 642-82.

RESULTS AND DISCUSSION

It appeared that the workability of the glasscrete in terms of the slump measurements were about 45–80 mm in non-reinforced cases and around 40-75 for polyamide EPS concretes. In addition, it should be noted that the mixes having the higher percentage silica fume can present higher slump values. During the experimental study, all the concretes specimens shown a interesting flexibility and provided a very easy condition to work with. Meanwhile, the specimens could be compacted using just hand compaction and they could be easily finished. In order to be able to solve the problems associated with the hydrophobic nature of the EPS beads, the silica fume and the superplasticizer were added. This will help to improve the cohesiveness of the mix significantly.

Figure 1 displays the development of compressive strength with the age for reinforced EPS concrete. This illustration clearly states that the compressive strength of reinforced EPS concrete in almost all mixes shows a continuous increase with age. It is seen that the rate of strength development was greater initially and decreased as the age increased. Comparison of strengths at 7 days revealed that non-reinforced concretes developed almost 40–50% of its 28-day strength. While it is seen that reinforced concretes developed almost 20–40% of the corresponding 28-day strength.

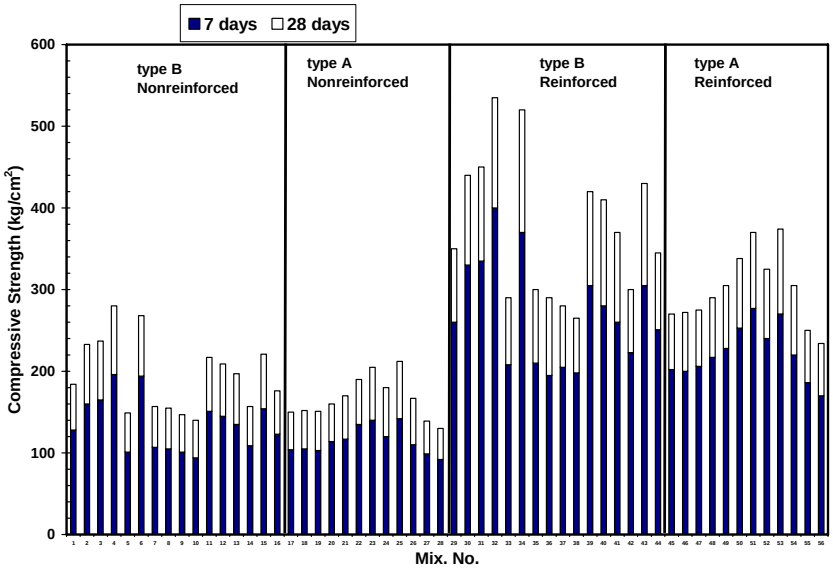

Figure 12. Effects of age on compressive strength.

Figures 2 and 3 illustrate the compressive strength of EPS concretes with different plastic densities for reinforced and non-reinforced concrete and the volume content of EPS.

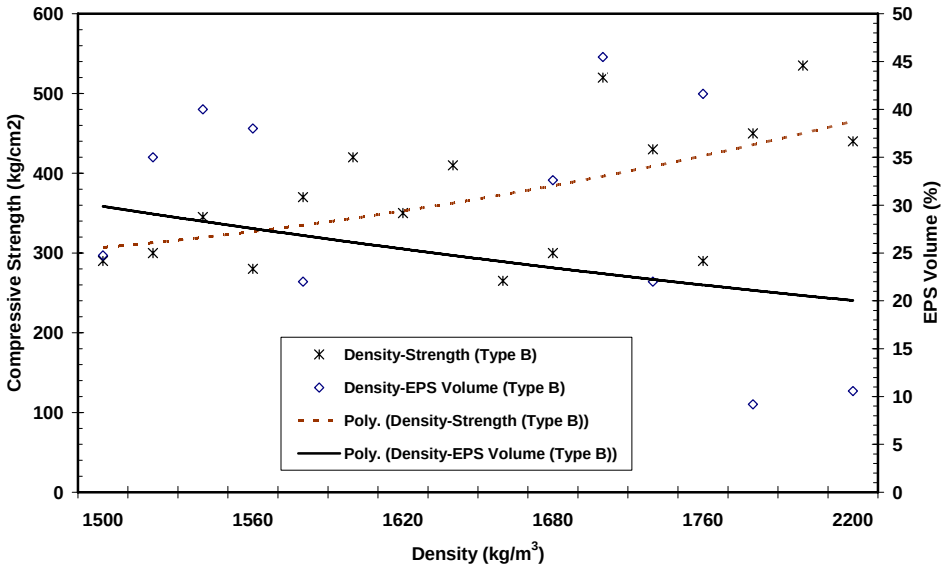

Figure 13. Variation of composite density with EPS volume and Compressive strength (type B).

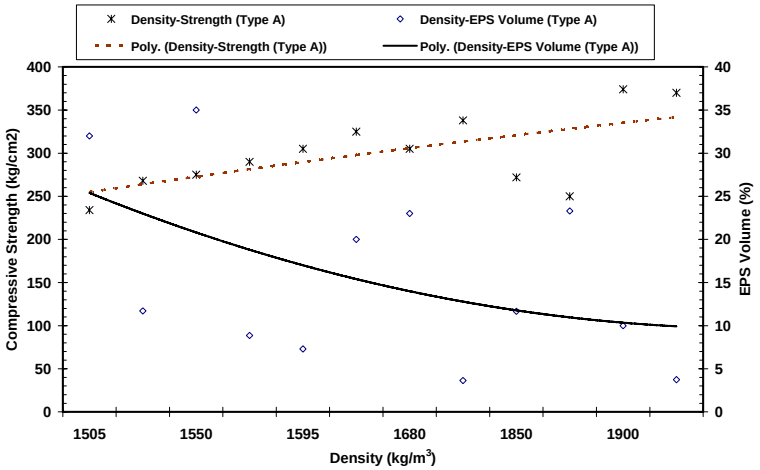

Figure 14. Variation of composite density with EPS volume and Compressive strength (type A).

It is appeared that the strength of non-reinforced and reinforced EPS concrete to increase linearly with a decrease in the EPS volume. Furthermore, it is noted that the density of EPS concretes decreased significantly with an increase in the EPS volume. It is clearly observed that the polyamide EPS concrete have high strength in compression, comparing to that non-reinforced concretes.

The plot represented in figure 4 show an inverse relationship between the concrete strength and the bead size. That means the strength in EPS concrete increased with a decrease in the EPS bead size for the same mix proportions.

From figure 5 it can be clearly appreciated that in the mixes content fine silica fume the compressive strength can increase significantly (i.e. mixes no. 4, 6,…). This represents the effects of fine silica fume and polyamide fiber on the compressive strength of EPS concrete. This is clearly visible that fine silica fume can improve the dispersion of EPS in the cement paste and interfacial bonding between EPS and cement paste. Moreover, the compressive strength of polyamide EPS concrete is almost 1.5 to 2 times non-reinforced EPS concretes.

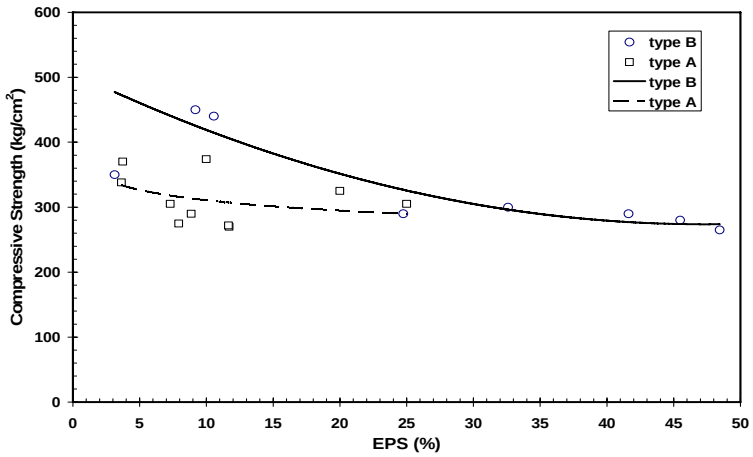

Figure 15. Effects of EPS bead size on compressive strength.

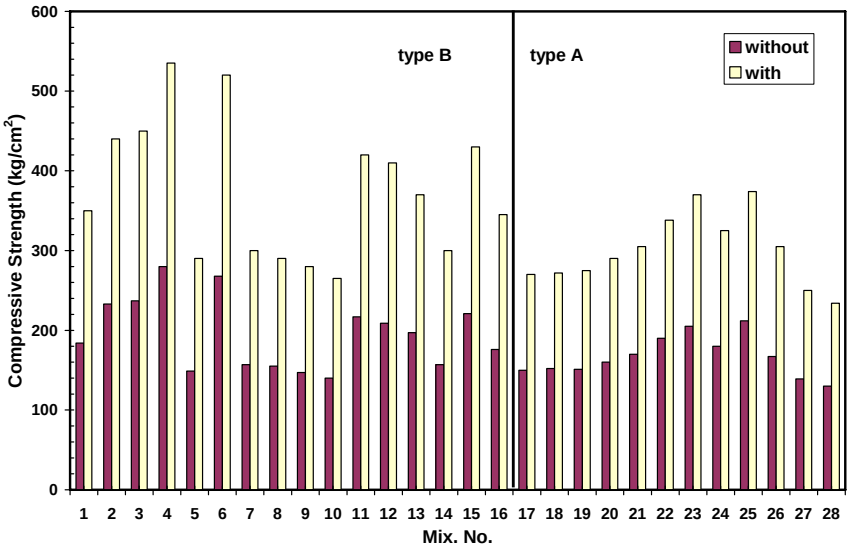

Figure 16. Effects of silica fume and polyamide on compressive strength.

The failure modes of different specimens are presented in figure 6. Figure (6a) shows the EPS concrete specimen before loading. The failure mode observed in figure (6b) is rather gradual (more compressible), and the specimen is capable of retaining the load after failure, without full disintegration. Figure (6c) illustrates failure mode in polymer concretes containing EPS with polyamide yarns. This is attributed to the fact that the failure mode of this specimen is near to a typical brittle failure.

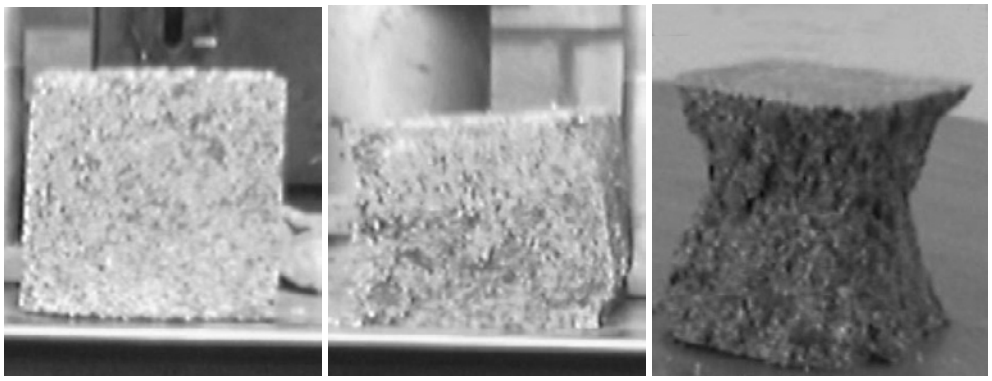

(a) (b) (c)

Figure 17. The EPS concrete samples with and without polyamide fibers; (a) Compressive samples before failure, (b) Observed failure mode in polymer concretes containing EPS without polyamide fibers and c) Observed failure mode in polymer concretes containing EPS with polyamide fibers.

Figure 7 illustrates the effects of volume content of EPS on the tensile strength of polyamide EPS concretes. This attribute shows the fact that there is an inverse relationship between the concrete tensile strength and the EPS volume. This means that the tensile strength of EPS concrete appeared to increase with a decrease in the EPS volume.

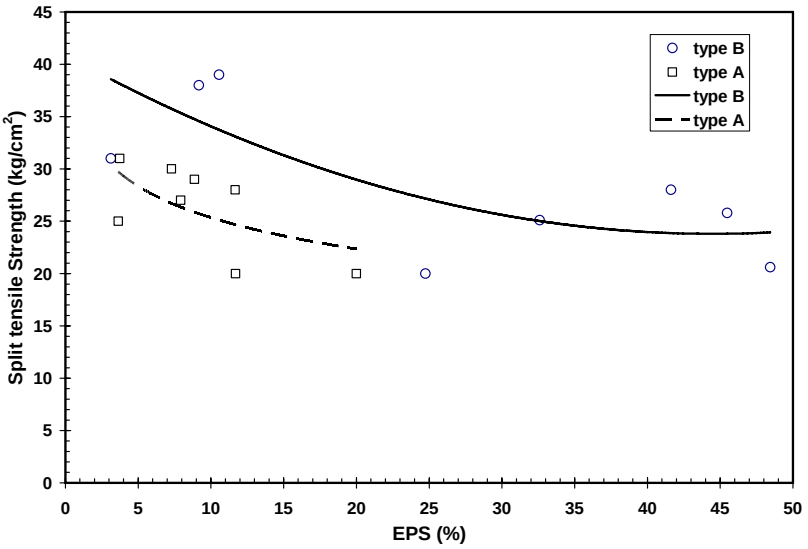

Figure 18. Variation of tensile strength with EPS volume.

From figure 8, the tensile strength of polyamide EPS concrete (type B) is 40 kg/cm2 whereas, the maximum tensile strength for polyamide EPS concrete (type A) is only 31 kg/cm2. But in general, we can expect an increase of 70% in the tensile strength for the lower bead sizes.

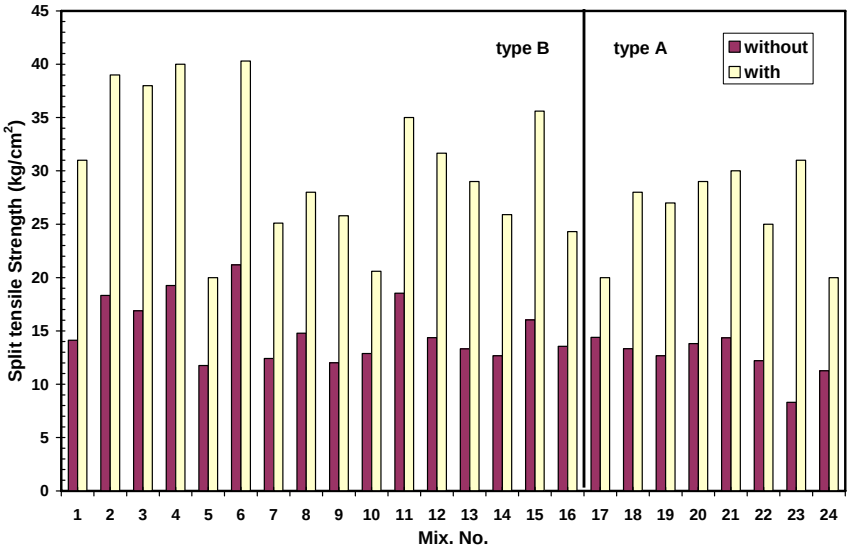

Figure 19. Effects of EPS bead size on tensile strength.

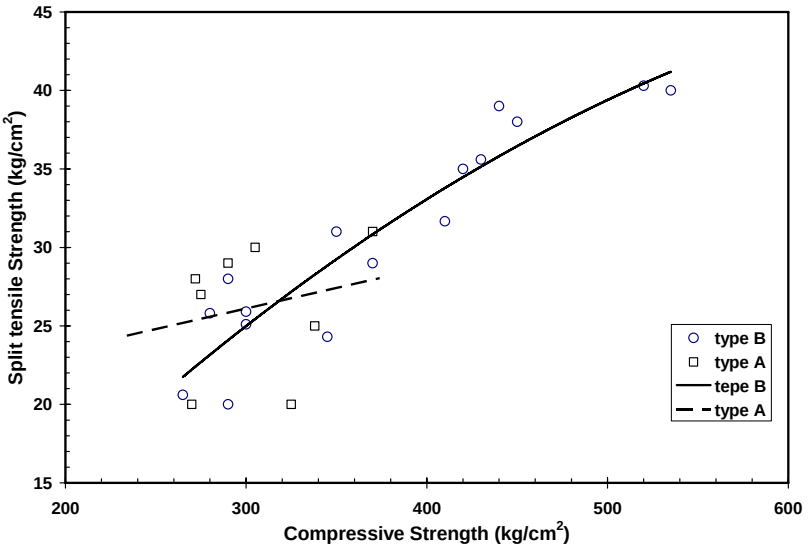

Figure 20. Variation of tensile strength with compressive strength.

Efforts were made to study the variation of tensile strength with the compressive strength (figure 9). It appears that the tensile strength increased with an increase in compressive strength. The rate of strength increasing in polyamide-EPS glasscrete containing small beads (type B) is higher than other.

The splitting failure mode of the concrete specimens containing non-reinforced EPS aggregates also did not exhibit the typical brittle failure principally expected in conventional concrete as in compressive strength. Consequently, the tensile failure mode observed in the polymer glasscrete containing polyamide fibers was rather a typical brittle failure which is normally resembles to conventional concrete (figure 10).

Figure 21. The failure mode in EPS glasscrete.

Shrinkage

The most significant factor affecting the shrinkage of concrete is the degree of restraint by the aggregate (i.e. its elastic properties and the volumetric proportion of the paste in the mix). It should be noted that the EPS beads principally offer little hindrance to the shrinkage of the paste. Therefore it is expected that as the volumetric proportion of the EPS is increased, the shrinkage would increase as well. This is clearly represented in figure 11. In this study, the drying shrinkage of normal concrete at 90 days was 610 microstrain. Inversely, when the volume content of EPS in the concrete specimen was 20%, the drying shrinkage at 90 days raised to 1000 microstrain, which represents a disadvantage for the application of EPS.

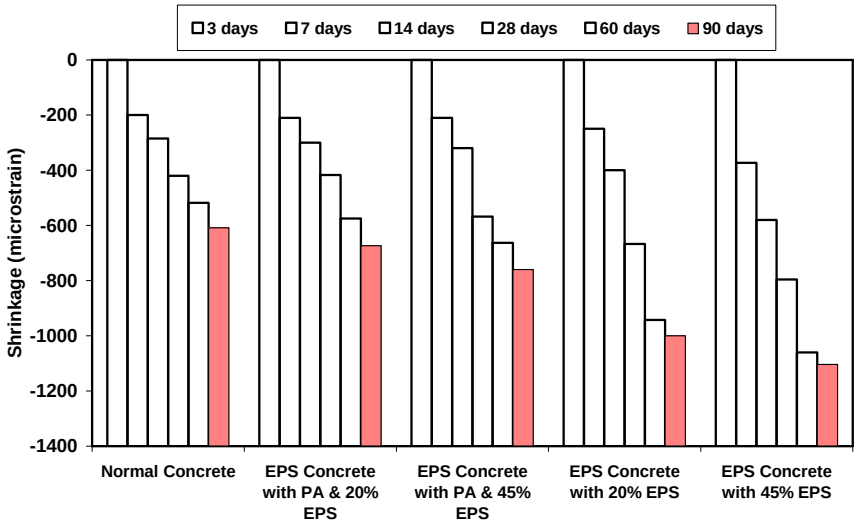

Figure 22. Relationship between drying shrinkage strain of EPS concrete (with polyamide and without polyamide) and reference concrete with age.

In a view of the above, it can be seen that polyamide yarns improved the drying shrinkage of EPS concrete significantly. Even for the case of EPS glasscrete which contained 20% of its volume by EPS, the drying shrinkage at 90 days was 670 microstrain, which seems to be rather close to normal concrete range.

CONCLUSION

The data presented in this paper show that there is a great potential for the utilization of waste glass and waste fibers in EPS concrete. It is considered this utilization would provide much greater opportunities for value adding and cost recovery as it could be used as a replacement for expensive materials.

The use of recycled materials in glasscrete has been on the increase throughout the world due to conserving resources. The results of this study have shown that use of this locally available low-cost PA waste may provide an economical and effective alternative to concrete aggregates.

REFERENCES

[1] M. Muthukumar and D. Mohsen, "Studies on polymer concrete based on optimized aggregate mix proportion", *European Polymer Journal*, Volume 40, 2004, pp. 2167-2177.

[2] J. P. Gorninski, D. C. Dal Mobin and C. S. Kazmierczak, Study of the modulus of elasticity of polymer concrete compounds and comparative assessment of polymer concrete and Portland cement concrete, *Cement and Concrete Research*, Volume 34, 2004, pp. 2091-2095.

[3] ACI Committee 213 R-87. Guide for Structural Lightweight Aggregate Concrete, ACI Manual of Concrete Practice, Part 1, American Concrete Institute, Farmington Hills (1987).

[4] A. Short and W. Kinniburgh, Lightweight Concrete. (3rd ed.),, *Applied Science Publishers*, London (1978).

[5] V. Sussman, Lightweight plastic aggregate concrete. *ACI J.* (1975 (July)), pp. 321–323.

[6] C. Bagon and S. Frondistou-Yannas, Marine floating concrete made with polystyrene expanded beads. *Mag. Concr. Res.* 28 (1976), pp. 225–229

[7] K. G. Babu and D. S. Babu, Behaviour of lightweight expanded polystyrene concrete containing silica fume, *Cement and Concrete Research*, Volume 33, Issue 5 , May 2003, pp. 755-762.

[8] A.A. Al-Manaseer and T.R. Dalal, Concrete containing plastic aggregates. *Concr. Int.* (1997 (August)), pp. 47–52.

[9] CEB-FIP. Diagnosis and assessment of concrete structures—State of the art report, CEB Bulletin 1989.

In: Monomers, Oligomers, Polymers, Composites… ISBN: 978-1-60456-877-6
Editors: R. A. Pethrick, G.E. Zaikov et al.

Chapter 17

ELECTROSPUN NANOFIBERS AND IMAGE ANALYSIS

M. Ziabari, V. Mottaghitalab and A. K. Haghi*
University of Guilan, P. O. Box 3756, Rasht, Iran

ABSTRACT

In the first part of this chapter electrospinning process of nanofiber is introduced. In the second part, a new image analysis technique for measuring the diameters of electrospun nanofibers is developed.

1.1. INTRODUCTION

When the diameters of polymer fiber materials are shrunk from micrometers (for example 10-100 μm) to sub-microns or nano meters (for example 10×10^{-3}-100×10^{-3} μm), there appear several amazing characteristics such as very large surface area to volume ratio, flexibility in surface functionalities, and superior mechanical performance compared with any other known form of material. These outstanding properties make the polymer nanofibers to be optimal candidates for many important applications. The electrospinning process is not a new technology for polymer fiber production seems to be the only method which can be further developed for mass production of one-by-one continuous nanofibers from various polymers. It has been known since the 1930's; however, it did not gain significant industrial importance due to the low output of the process, inconsistent and low molecular orientation, poor mechanical properties and high diameter distribution of the electrospun fibers. Although special needs of military, medical and filtration applications have stimulated recent studies and renewed interest in the process, quantitative technical and scientific information regarding process and product characterization are extremely limited. Electrospinning has gained renewed interest as a method to produce ultra-thin fibers with diameters in the

* Corresponding author E-Mail: Haghi@Guilan.ac.ir

nanometer to micrometer scale range. Nanofibers exhibit special properties mainly due to extremely high surface to weifht ratio compared to conventional nonwovens [1-4]. Low density, large area to mass, high pore volume, and tight pore size make the nanofiber nonwoven appropriate for a wide range of the filtration applications. Figure 1 shows how much smaller nanofibers are compared to a human hair, which is 50-150 μm.

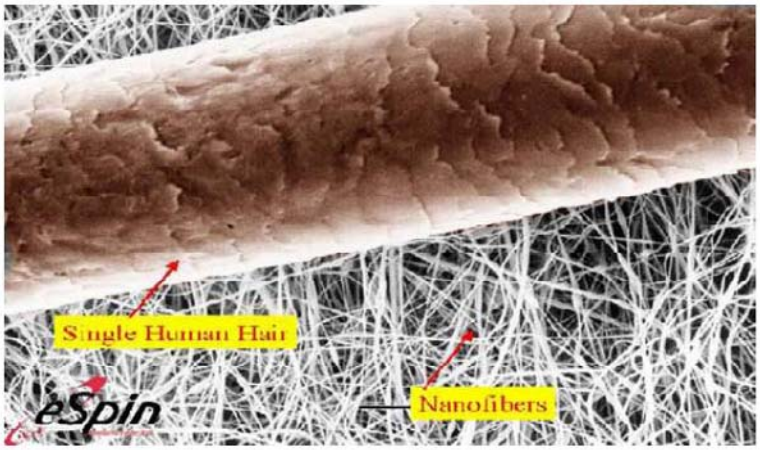

Figure 1. Comparison between human hair and nanofiber web.

Nanofibers have significant applications in the area of filtration since their surface area is substantially greater and have smaller micropores than melt blown (MB) webs. High porous structure with high surface area makes them ideally suited for many filtration applications. Nanofibers are ideally suited for filtering submicron particles from air or water. Electrospun fibers have diameters three or more times smaller than that of MB fibers. This leads to a corresponding increase in surface area and decrease in basis weight. Table 1 shows the fiber surface area per mass of nanofiber material compared to MB and SB fibers.

Table 1. Fiber surface area per mass of fiber material for different fiber size

Fiber Type	Fiber size, in Micrometer	Fiber surface area per mass of fiber material m2/g
Nanofibers	0.05	80
Spunbond fiber	20	0.2
Melt blown fiber	2.0	2

Nanofibers are widely used in medical applications, which include, drug and gene delivery, artificial blood vessels, artificial organs, and medical facemasks. For example, carbon fiber hollow nano tubes, smaller than blood cells, have potential to carry drugs in to blood cells (for more information refer to: www.donaldson.com , www.ecmjournal.org and www.zapmeta.com). A Comparison of red blood cell with nanofibers web is shown in figure 2. With electrospaun fibers we can even make bandages that are absorbed by the body (figure 3).

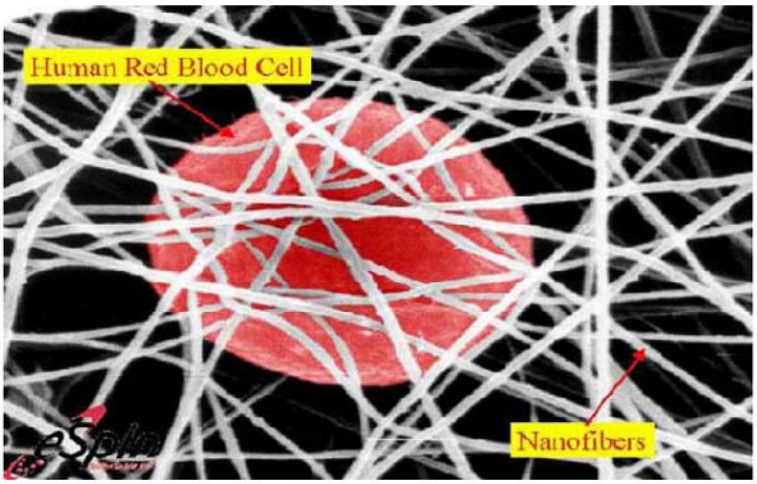

Figure 2. Comparison of red blood cell with nanofibers web.

Figure 3. Photograph of a cotton gauze (left) and an electrospun bovine fibrinogen mat (right) produced from 0.167 g/ml fibrinogen in HFP/MEM that is approximately 6 x 6 cm with a thickness of 0.7 mm (dry mass is approximately 0.08 grams) for potential use as a tissue engineering scaffold or wound dressing.

Electrospinning is a fiber spinning technique driven by a high-voltage electrostatic field using polymeric solution or liquid that produces polymer nanofibers. The variables controlling the behavior of the electrified fluid jet during electrospinning can be divided into fluid properties and operating parameters. The relevant fluid properties are viscosity, conductivity, dielectric constant, boiling point, and surface tension. The operating parameters are flow rate, applied electric potential, and the distance between the tip and the collector called air gap.

Electrospinning is a method of producing nanofibers by accelerating a jet of charged polymer solution in an electric field (figures 4 and 5). A high-voltage generator generates an electric field between syringe with a capillary tip and grounded collector. A polymer solution is charged by the high-voltage generator and is ejected from the capillary tip. The grounded collector can be a screen or rotating drum and is placed at a fixed distance from the capillary

tip. The ejected polymer solution forms a so-called "Taylor cone" at the end of the tip and is drawn toward the grounded collector. During the motion of the jet in traveling to the collector, the solvent evaporates and deposits a non-woven fiber mat on the collector. Homogeneously dissolved polymer solution can be taken in the glass syringe and mounted on the syringe pump. Initially, the polymer solution is held by its surface tension in the form of a droplet at the end of the capillary tip. The positive electrode from the high voltage source should be connected to the syringe needle tip by means of an alligator clip. The negative terminal of the power source and the collector screen should be grounded. As the voltage is increased, the droplet becomes distorted by the induced electrical charge on the liquid surface, and a stable jet of polymer solution is then ejected from the cone. Above a given critical voltage, the jet breaks up into droplets as a result of surface tension. The final products of fibers and beads are determined by the electrospinning parameters. The break-up of the jet depends on the magnitude of the applied electric current. The more electric current the jet carries, the less likely it is to form droplets. A higher net charge density of the polymer solution could, therefore, yield thinner fibers with no beads (figures 6-8). Nanofibres can be collected on a smooth aluminum foil.

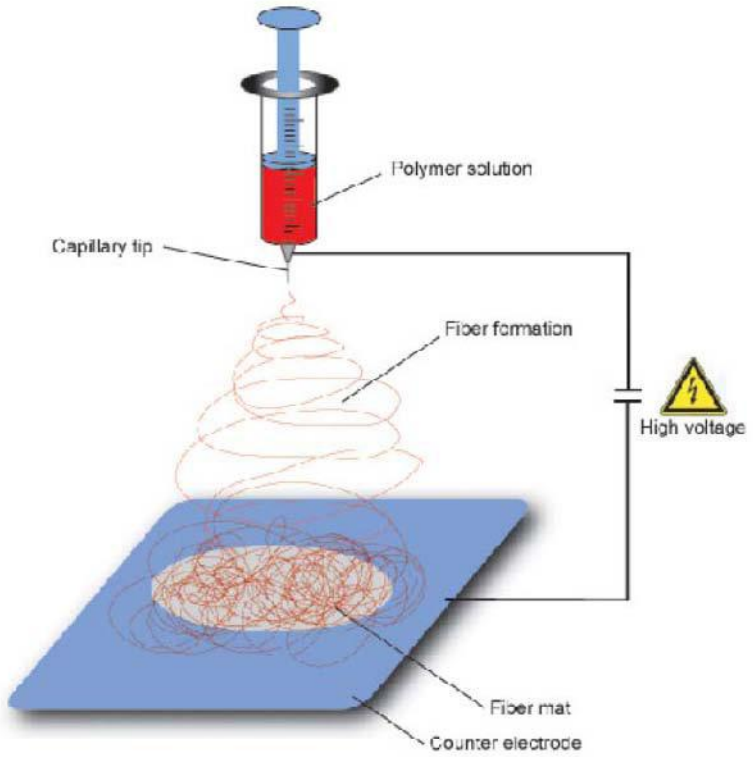

Figure 4. Electrospinning process.

The uniformity and non-uniformity in structure of nanofibers spun can be characterized using Scanning Electron Microscopy (SEM) as it is shown in figure 9. The morphology of nanofibres spun can be characterized using Atomic Force Microscopy (AFM). Sample preparation for the SEM characterization requires the usage of sputter coater. The samples to

be analyzed should be placed over a carbon tape on an aluminum pedestal and sputter coated with gold-platinum alloy to a thickness of 200Ao-300Ao.Surface morphology of the nanofibre samples can be characterized using the AFM images. Structure and morphology of nanofibres produced by the electrospinning process depends on the process parameters like the applied voltage, needle tip-collector distance, solution concentration and conductivity and solvent volatility. Other parameters like needle tip or capillary diameter, surrounding gas stream, conductivity of the collector screen, etc. could also influence the fiber morphology and orientation.

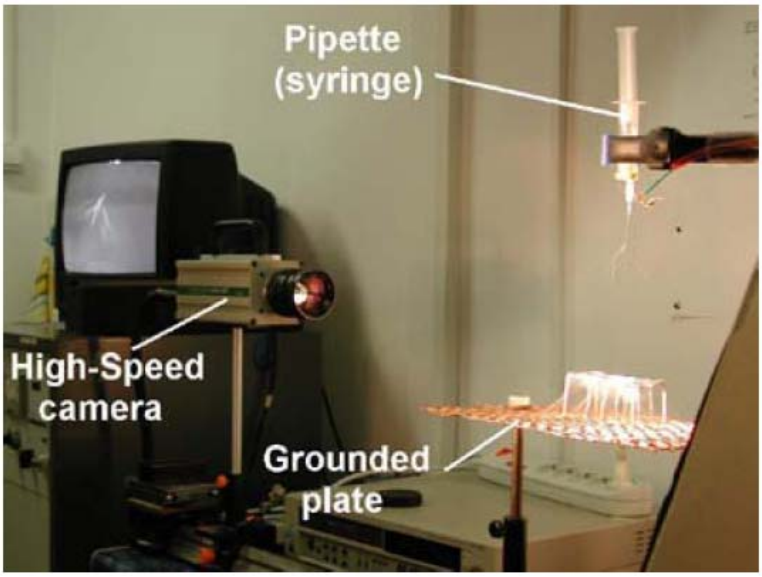

Figure 5. Photo of the experimental setup of the electrospinning process.

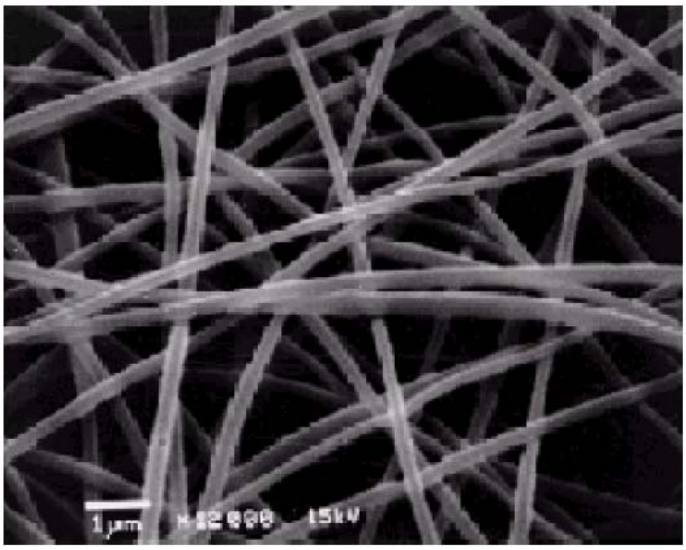

Figure 6. SEM Photograph of Electrospun Polyacrylonitrile Fiber.

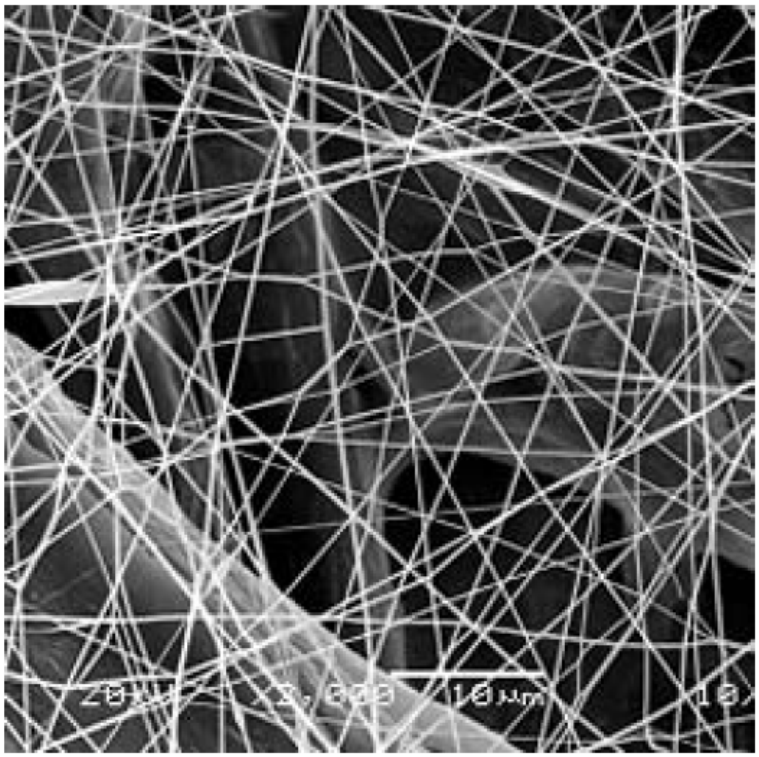

Figure 7. A typical SEM images of electrospun nanofibers.

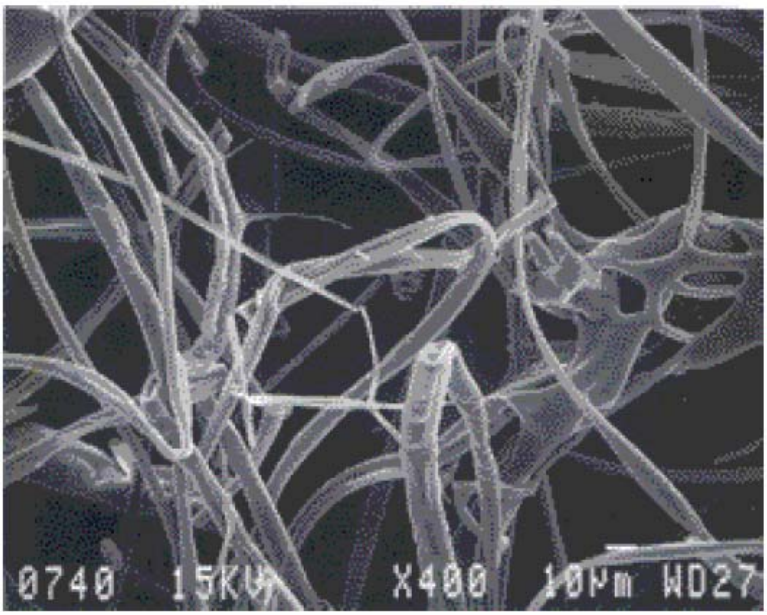

Figure 8. A typical SEM images of electrospun nanofibers.

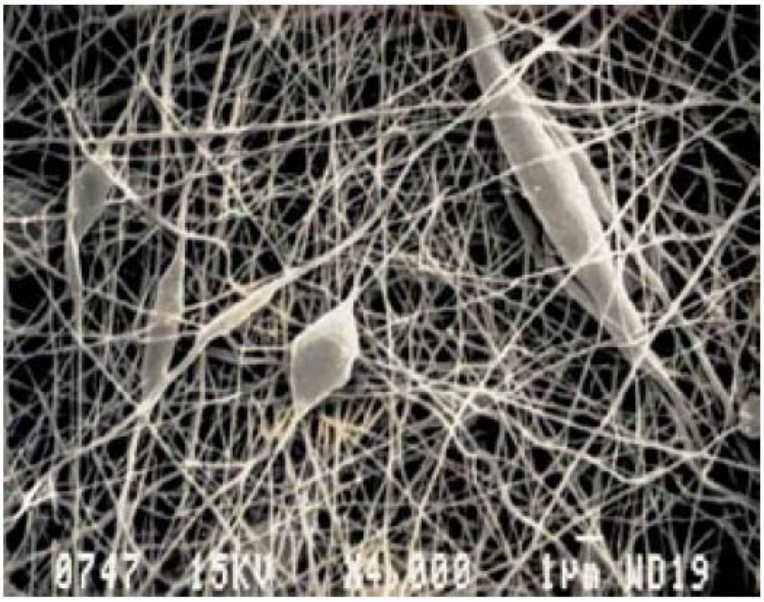

Figure 9. SEM images of nonuniform electrospun nanofibers.

In figure 8 it can be seen that how for certain experiments that we are collecting electrospun fibers onto an insulating film we can measure the charge to mass ratio by NanoCoulomb Meter.

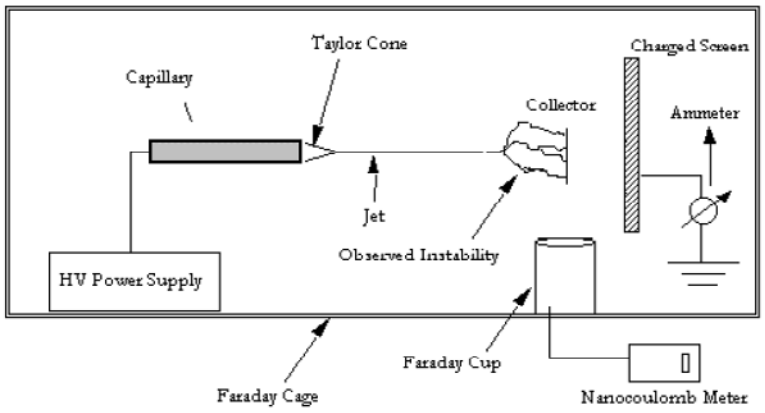

Figure 10. Charge Measurement Setup.

1.2. POLYMER-SOLVENTS USED IN ELECTROSPINNING

The polymer is usually dissolved in suitable solvent and spun from solution. Nanofibers in the range of 10-to 2000 nm diameter can be achieved by choosing the appropriate polymer solvent system. Table 2 gives list of some of polymer solvent systems used in electrospinning.

Table 2. Polymer solvent systems for electrospinning

Polymer	Solvents
Nylon 6 and nylon 66	Formic Acid
Polyacrylonitrile	Dimethyl formaldehyde
PET	Trifluoroacetic acid/Dimethyl chloride
PVA	Water
Polystyrene	DMF/Toluene
Nylon-6-co-polyamide	Formic acid
Polybenzimidazole	Dimethyl acetamide
Polyramide	Sulfuric acid
Polyimides	Phenol

1.3. QUANTITIVE ANALYSIS OF ELECTROSPINNING PROCESS

Quantitive analysis of the electrospinning process consists of the following:

- *Solution properties*. The relevant fluid properties are density, viscosity, surface tension, permittivity, conductivity and viscoelasticity. Of these, viscosity and conductivity appear to play the greatest role in the electrospinning of dilute solutions.
- *Operating parameters*. The relevant operating parameters are flow rate, electric field strength, and electric current flow between the spinnerette and collector. The volumetric flow rate is closely controlled through the use of the syringe pump. Field strength may be varied by changing either the applied voltage or the distance over which the voltage drop to ground occurs.
- *Online process monitoring*. Macrophotography is used to image the thinning of the fluid jet as it leaves the spinnerette.
- *Fiber characterization.* Fiber diameter distributions are measured using scanning electron microscopy.

1.4. POLYMERIC NANOCOMPOSITES

Polymeric nanocomposites made by incorporating small amount of nanoscale inclusions into polymer matrices exhibit dramatic changes in thermomechanical properties over the pure polymers. Because the properties of the nanoscale fillers can be extraordinary, even small volume fractions can result in significant changes. Enhancing the effect is the extremely significant role that the interphase plays in these systems. Given the enormous surface to volume ratio for nanoparticles, the interphase volume fraction can dwarf that of the inclusions themselves. Nanocomposites are a new class of composites, that are particle-filled polymers for which at least one dimension of the dispersed particles is in the nanometer range. Over the last decade, the utility of layered silicate nanoparticles as additives to enhance polymer performance has been established. Nanoscale fillers result in physical behaviour that is

dramatically different from that observed for conventional microscale counterparts. For instance, increased moduli, gas barrier, increased strength and reduced thermal expansion coefficients are observed with only a few percent additions of nanofiller; thus maintaining polymeric processability, cost and clarity.

The reinforcement of polymers using fillers, whether inorganic or organic, is common in the production of modern plastics. Polymeric nanocomposites (PNCs) (or polymer nanostructured materials) represent a radical alternative to conventional-filled polymers or polymer blends. In contrast to the conventional systems where the reinforcement is on the order of microns, discrete constituents on the order of a few nanometers (~10,000 times finer than a human hair) exemplify PNCs.

Uniform dispersion of these nanoscopically sized filler particles (or nanoelements) produces ultra-large interfacial area per volume between the nanoelement and host polymer. This immense internal interfacial area and the nanoscopic dimensions between nanoelements fundamentally differentiate PNCs from traditional composites and filled plastics. Thus, new combinations of properties derived from the nanoscale structure of PNCs provide opportunities to circumvent traditional performance trade-offs associated with conventional reinforced plastics, epitomizing the promise of nano-engineered materials.

Main feature of polymeric nanocomposite, in contrast to conventional composites, is the reinforcement is on the order of nanometer deeply affected final macroscopic properties.

Several types of polymeric nanocomposites can be obtained with different particle nanosize, nature and shape, such as clay/polymer nanocomposites, and metal/polymer nanocomposites.

Nanocomposites have been formed with a wide variety of polymers including: epoxy, polyurethane, polyetherimide, poybenzoxazine, polypropylene, polystyrene, polymethyl methacrylate, polycaprolactone, polyacrylontrile, polyvinyl pyrrolidone, polyethylene glycol, polyvinylidene fluoride, polybutadiene, copolymers and liquid crystalline polymers.

1.4.1. Clay/Polymer Nanocomposites

Clay is a natural material that has been used by man from ancient times in pottery and building materials. Common clays are naturally occurring minerals and are thus subject to natural variability in their constitution. The purity of the clay can affect final nanocomposite properties. Many clays are aluminosilicates, which have a sheet-like (layered) structure, and consist of silica SiO_4 tetrahedra bonded to alumina AlO_6 octahedra in a variety of ways. A 2:1 ratio of the tetrahedra to the octahedra results in smectite clays, the most common of which is montmorillonite. Other metals such as magnesium may replace the aluminium in the crystal structure. Depending on the precise chemical composition of the clay, the sheets bear a charge on the surface and edges, this charge being balanced by counter-ions, which reside in part in the inter-layer spacing of the clay. The thickness of the layers (platelets) is of the order of 1 nm and aspect ratios are high, typically 100-1500. The clay platelets are truly nanoparticulate. In the context of nanocomposites, it is important to note that the molecular weight of the platelets *(*ca. 1.3×10^8) is considerably greater than that of typical commercial polymers, a feature which is often misrepresented in schematic diagrams of clay-based nanocomposites. In addition, platelets are not totally rigid, but have a degree of flexibility. The clays often have very high surface areas, up to hundreds of m^2 per gram. The clays are also characterised

by their ion (e.g. cation) exchange capacities, which can vary widely. One important consequence of the charged nature of the clays is that they are generally highly hydrophilic species and therefore naturally incompatible with a wide range of polymer types. A necessary prerequisite for successful formation of polymer-clay nanocomposites is therefore alteration of the clay polarity to make the clay 'organophilic'. An organophilic clay can be produced from a normally hydrophilic clay by ion exchange with an organic cation such as an alkylammonium ion. For example, in montmorillonite, the sodium ions in the clay can be exchanged for an amino acid such as 12-aminododecanoic acid (ADA):

$$Na^{+}\text{-CLAY} + HO_2C\text{-R-}NH_3^{+}Cl^{-} \rightarrow .HO_2C\text{-R-}NH_3^{+}\text{-CLAY} + NaCl$$

Clay can be described as being a layered material. In layered materials the bonds between the atoms in the layer are very strong, but the bonds between the layers are much weaker. This enables the layers to be easily separated. Figure 11 shows the structure of a typical clay layer.

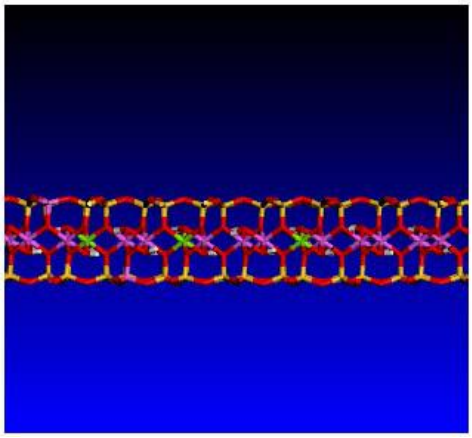

Figure 11. Structure of a typical clay layer.

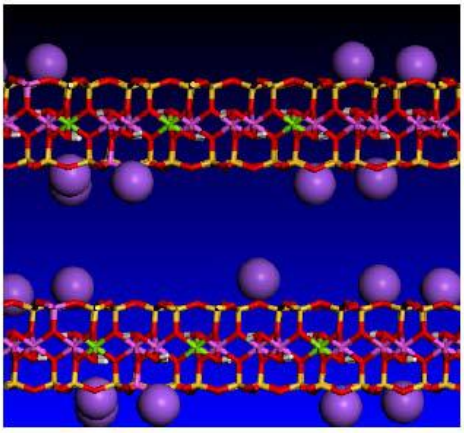

Figure 12. Sheets stack on top of one another.

The clay sheet shown consists of three sub-units: a octahedral center layer consisting of mainly aluminium (Al) cations; two tetrahedral layers consisting mainly of silica (Si) and oxygen (O) atoms. In the octahedral layer some of the Al^{3+} atoms are subsituted by magnesium^{2+} atoms which gives rise to a net negative charge on the layer. Similarly, some of the Si^{4+} may be substituted by Al^{3+} resulting in negative charge in the tetrahedral layers.

Figure 12 shows how the clay sheets stack on top of one another. The resulting negative charge has to be counter-balanced by the introduction of positive ions (cations) in the region between the clay sheets (interlayer or gallery) and at the clay surface. The amount of charge on the clay layer is known as the Cation Exchange Capacity of the clay. In natural clays the charge balancing cations are mainly Na^{+}, K^{+} and Ca^{2+}. These cations tend to have water molecules associated with them in the interlayer region, a fact which makes clay soils swell in wet weather and shrink or crack in dry weather.

It is also possible to incorporate other molecules into the interlayer regions of the clay system. These molecules may be charged or neutral. Charged molecules, such as organo-ammonium species are incorporated by exchanging them for the small inorganic cations - a process known as cation exchange. Neutral molecules may also be intercalated into the clay through favourable entropic and enthalpic interactions. This enables the uptake of molecules such as poly(ethylene glygol) and related species, phenols, etc. Often water is displaced from the clay interlayer during this process. An example of a clay-polymer system is shown in figure 13.

When a clay-polymer nanocomposite is formed there are three ways in which the clay can be incorporated in the polymer. Figure 14 is a simple schematic showing the 3 forms.

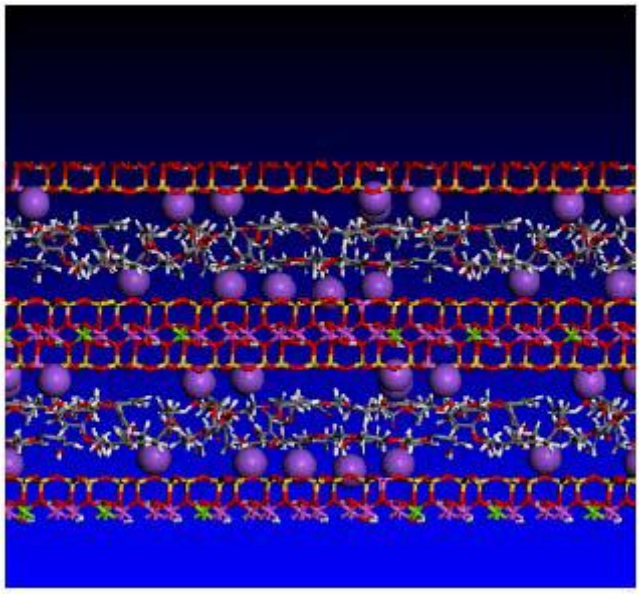

Figure 13. Clay-polymer system.

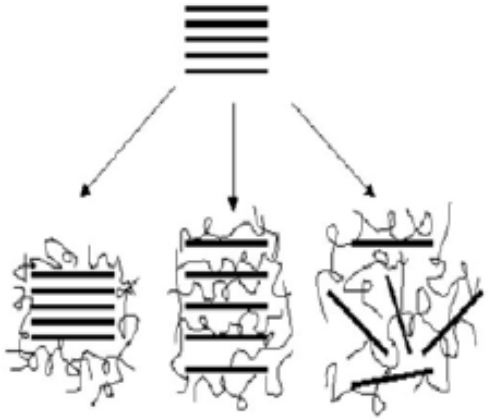

Figure 14. Clay-polymer nanocomposite.

In figure 14a the clay layers do not separate and the clay tactoid is incorporated wholly within the polymer. At the other extreme, figure 14c shows a fully exfoliated clay where all the layers are separated and incorporated within the polymer as individual sheets. Figure 14b shows an intercalated clay, where the clay sheets have separated enough to let some polymer between the sheets, but still retain the layered structure.

When low levels of clay are added to a polymer it is desirable to fully exfoliate the clay so that an even (homogeneous) distribution of clay sheets through the polymer is achieved.

Metal-polymer nanocomposites are obtained using nano-particles (nanostructured metal)as additives in polymer matrix. Nano-sized metals has different properties from bulk metals originating from nanocrystals size. Nanocrystals measure a few nanometers containing few hundred atoms. In this way, nanomaterials shows unique properties (electronic, magnetic, structural) depending on nano-size structure.

Physical and chemical properties of metal nanoparticles are as follow:

The specific-size dependence of these properties becomes evident when they:

- no longer follow classical physical laws but rather are described by quantum mechanical ones;
- are dominated by particular interface effects;
- exhibit properties due to a limited number of constituents, since the usual term "material";

2.1. IMAGE ANALYSIS

An image analysis based method was proposed by Pourdeyhimi et al. [5] for measuring fiber diameter in nonwoven textiles. In this method, a binary image of the textile is used to create a distance map and skeleton. The fiber diameter may be determined from the values of the distance map at any pixel location on the skeleton. However, the occurrence of a broken skeleton at intersection points is a main challenging area within the use of this method. Since two or more fibers cross each other at these intersections, the value of the center of the object

in the distance map doesn't coincide with the fiber diameter at these points because it isn't associated with a single fiber. The problem becomes more serious as fibers get thicker and for points where more fibers cross each other. Hence, the method fails in measuring fiber diameter at intersections.

2.2.1. New Distance Transform Algorithm

We established a new method based on image analysis in which the problem associated with the intersections was solved. The method uses a binary image as an input. Then, the distance transformed image and the skeleton are created. It can be noted that the skeleton which is obtained by the process of *skeletonization* or *thinning* often contains short spurs which may be cleaned up through the use of a *pruning* procedure [2]. In order to solve the problems associated with measuring fiber diameter at the intersections, we first use a *sliding neighborhood* operation [6] to identify the location of these points. Then the thickness of each intersection is recorded from the distance transformed image. Finally the intersections are deleted from the skeleton image based on their measured thickness.

Figure 15 shows a simple simulated web and the resulting skeleton superimposed on the distance transformed image. The obtained skeleton is used as a guide for tracking the distance transformed image and the diameters are computed from the intensities of this image at all points along the skeleton. The data in pixels may then be converted to *nm* and the histogram of fiber diameter distribution is plotted.

2.2.2. Web Simulation

In order to validate the method, test samples with known characteristics were required. Algorithms for simulation of nonwoven mats have been proposed by Abdel-Ghani et al. [3] and Pourdeyhimi et al. [4]. Lately it has been discovered that the best way to simulate nonwoven mats of continuous fibers is through *μ-randomness* procedure [8] which was used in this study for generating a simulated image with known characteristics.

2.2.3. Real Web Treatment

Fiber diameter determination by the use of image analysis requires the initial segmentation of the micrographs in order to produce binary images. The typical way of producing a binary image from a grayscale image is by *global thresholding* [5, 6] where a single constant threshold, usually selected by trial and error, is applied to segment the image. Global thresholding is very sensitive to any inhomogeneities in the gray-level distributions of the object and background pixels. This effect can be eliminated through the use of a *local thresholding* [7, 8] scheme. Automatic selection of the appropriate thresholds can be carried out based on, *Otsu's method* [9]. Note that, since the process is extremely sensitive to noise, before the segmentation, a procedure to clean the noise and enhance the contrast of the image is necessary.

3. RESULTS AND DISCUSSION

A simulated image with the diameter sampled from a normal distribution with the mean (M) of 15 and standard deviation (STD) of 4 pixels was used to test the validity of the method. It is noteworthy that the true M and STD of the simulated image (15.35 and 4.47) varies slightly with those used as simulation parameters.

Figure 16 shows the simulated image and its diameter distribution obtained from the new distance transform method. The M and STD of fiber diameter obtained by this method were 15.02 and 4.80 respectively, showing a good correlation between the calculated and true M and STD of the simulated image.

Using this method, there can be up to half a pixel error in either direction when measuring the fiber diameter, resulting in a total measurement error of up to 1-pixel. The slight differences observed between the calculated and true values could be attributed to this 1-pixel measurement error, some parts of branches remaining after pruning and other slight variations in the skeleton adjacent to the deleted intersections. Furthermore, the fiber diameters at the deleted intersections were not counted within the measurement and may contribute slightly to the variation observed.

To prove that this process is suitable for determination of fiber diameter on real samples, a real nanofiber web was obtained from electrospinning of polyvinyl alcohol (PVA) with average molecular weight of 72000 g/mol (MERCK). The micrograph of the electrospun web (figure 17a), was taken using a Philips (XL-30) Environmental Scanning Electron Microscope after gold sputter coating.

Figure 17b shows the diameter distribution for the real web. The respective M and STD of the fiber diameter obtained by this new method were 24.74 and 3.85 in terms of pixel and 323.7 and 50.4 in term of *nm* which are in good agreement with the values 24.36 and 3.19 pixels and 318.7 and 41.8 *nm* obtained from manual methods. The differences here can also be attributed to the different number of measurements taken between the methods used (over 2000 for our method versus 100 for the manual method). Nevertheless, in each case presented, the difference observed was within 1-pixel measurement error suggesting the main limitation with the process is with the resolution of the taken image.

4. CONCLUSION

In this study, a new image analysis based method for assessing nanofibers diameters was successfully developed. The validity of the method was tested using a simulated image as well as an image of a real electrospun nanofiber web. In the case of the real web, local thresholding was applied on the micrograph of the web taken from SEM to attain the necessary binary image. The M and STD of fiber diameter which were obtained using this new method were extremely close to true values on the simulated image. For the real web, M and STD of fiber diameter measured by the method were also in good agreement with those obtained from the manual method. The results show the effectiveness of the method for diameter measurement. The method is automated, accurate, and much faster than manual method and has the capability of being used as an on-line technique for quality control.

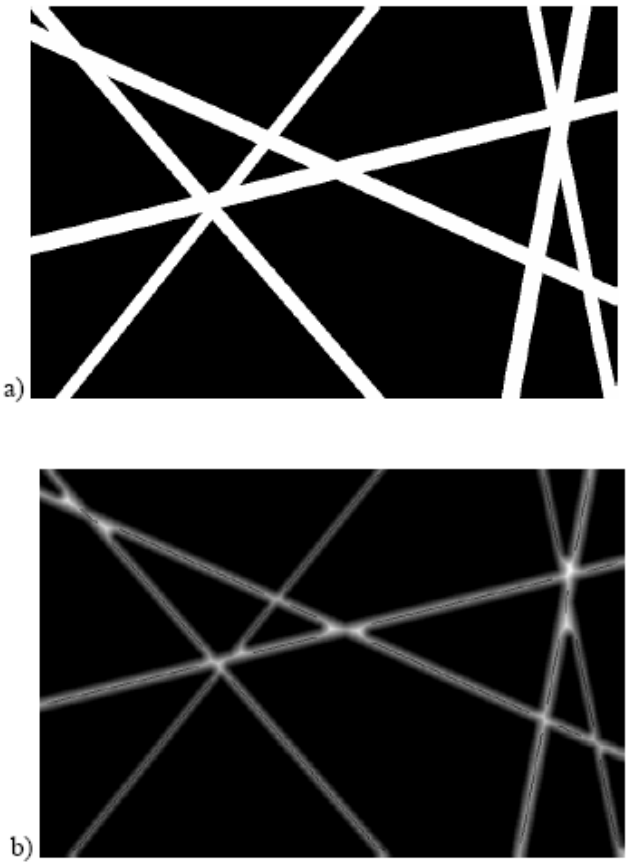

Figure 15. a) A simple simulated image, b) Resulting skeleton overlaid on distance transformed image.

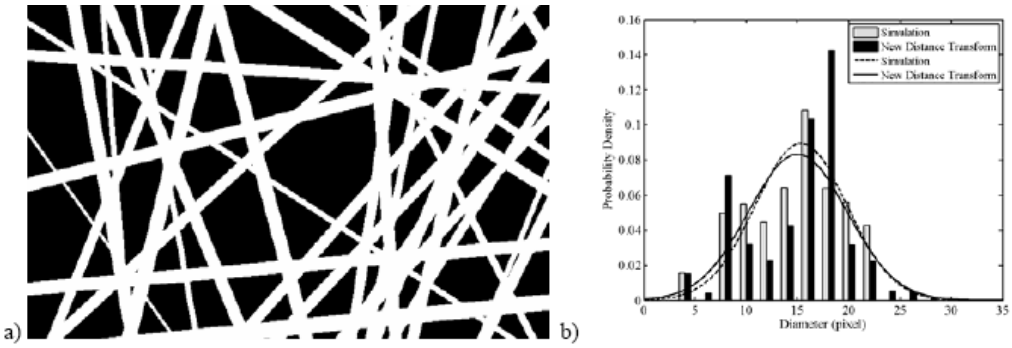

Figure 16. a) A simulated image, b) Its diameter distribution.

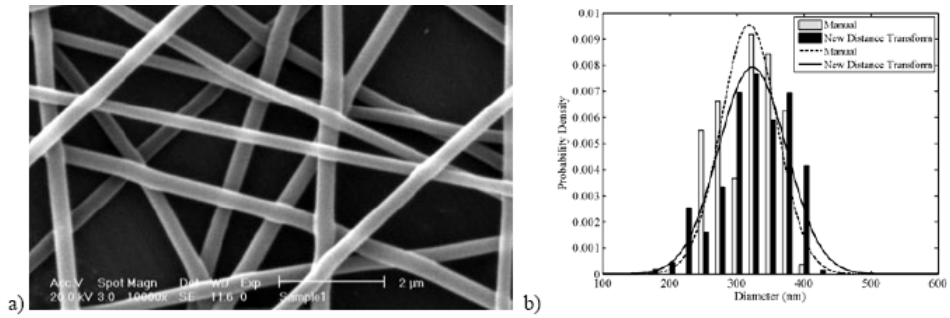

Figure 17. a) Micrographs of an electrospun web, b) Its diameter distribution.

REFERENCES

[1] A. K. Haghi, M. Akbari, *Phys. Stat. Sol.* (a) 204, 1830 (2007).

[2] D. H. Reneker, I. Chun, *Nanotechnology.* 7, 216 (1996).

[3] H. Fong, D. H. Reneker, Electrospinning and the Formation of Nanofibers, in: Structure Formation in polymeric Fibers, ed. by D. R. Salem (Hanser, Cincinnati, 2001), chap. 6, pp. 225-246.

[4] Th. Subbiah, G. S. Bhat, R. W. Tock, S. Parameswaran, S. S. Ramkumar, *J. Appl. Polym. Sci.* 96, 557 (2005).

[5] B. Pourdeyhimi, R. Dent, *Text. Res. J.* 69, 233 (1999).

[6] R. C. Gonzalez, R. E. Woods , Digital Image Processing (Prentice Hall, Second Edition, New Jersey, 2001).

[7] M. S. Abdel-Ghani, G. A. Davis, *Chem. Eng. Sci.* 40, 117 (1985).

[8] B. Pourdeyhimi, R. Ramanathan, R. Dent, *Text. Res. J.* 66, 713 (1996).

[9] M. Petrou, P. Bosdogianni, Image Processing the Fundamentals (John Wiley and Sons, England, 1999).

In: Monomers, Oligomers, Polymers, Composites… ISBN: 978-1-60456-877-6
Editors: R. A. Pethrick, G.E. Zaikov et al.

Chapter 18

INDUSTRIAL DRYING OF WOOD: TECHNOLOGY LIMITATION AND FUTURE TRENDS

A.K. Haghi**[*] **and R. K. Haghi
University of Guilan, P. O. Box 3756, Rasht, Iran

ABSTRACT

In this paper, a comprehensive review is presented on the researches and developments related to drying processes of wood. Other issues regarding the technology limitation, research challenges, and future trends are also discussed.

LIST OF SYMBOLS

A, B,	constants
Bi	Biot number for moisture loss
d_h	hydraulic diameter
D	moisture diffusivity
f_D	friction factor from Moody chart
F_O	Fourier number for moisture loss
k	moisture transfer coefficient,
L	half thickness, m
Re	Reynolds number
t	time
u_m	average speed
W	moisture content

[*] Corresponding author e-mail: Haghi@Guilan.ac.ir

ϕ	moisture content difference
Φ	dimensionless moisture content
μ	root of the transcendental characteristic equation
ρ	mass density of fluid
ν	Newtonian fluid viscosity
σ	surface roughness
Γ	dimensionless distance

1. INTRODUCTION

Porous materials such as wood have microscopic capillaries and pores which cause a mixture of transfer mechanisms to occur simultaneously when subjected to heating. Transfer of vapor and liquids occurs in porous bodies in the form of diffusion. In essence, transfer of liquids can occur by means of diffusion arising from hydrostatic pressure gradient. Heat and mass transfer in porous media is a complicated phenomenon and a typical case is the drying of moist porous materials. Scheidegger [1] claimed 47 years ago that the structure of porous media is too complex to be described precisely either in macro-scale or micro-scale, not to mention the combination of water with matrix. To date, there is no credible work proving that Scheidegger was wrong.

Convective drying is usually encountered in wood industry. The study of this type of drying has attracted the attention of several authors. Among the works relating to this question we cite the works of Plumb et al [2] and Basilico and Martin [3]. Convective drying of timber is one of the oldest and time-consuming methods to prepare the wood for painting and chemical treatments. The drying method can obviously have significant effect on the mechanical properties of wood. Major disadvantages of hot air drying are low energy efficiency and lengthy drying time during the falling rate period. The desired to achieve fast thermal processing has resulted in the increasing use of radiation heating. In this case, not only the removal of moisture is accelerated but also a smaller floor space is required, as compared to conventional heating and drying equipment.

It has also been recognized that dielectric heating could perform a useful function in drying of porous materials in the leveling out moisture profiles across wet sample. This is not surprising because water is more reactive than any other material to dielectric heating so that water removal is accelerated. This leads to giving a temperature gradient inside the wood sample with opposite directions to that in conventional drying processes. The Fickian diffusion theory for wood results in a mass transfer coefficient (surface emission factor) which is not in accordance with classical heat and mass transfer boundary layer theory. The mass transfer coefficient is one order of a magnitude lower than the ones obtained from classical theory. Checking susceptibility is closely related to stress development across the grain during drying. The tension stress at the beginning of the drying period develops rapidly causing a creep response of the surface. This mechanosorptive creep relaxes the tension stress enough to prevent checking in many cases. This effect is more pronounced at elevated temperatures. It is shown that high density and low temperature make wood more susceptible to checking, a property closely related to the value of strain at failure. Warping during drying is generally caused by the anisotropic shrinkage of wood. The study of cupping shows that it

depends mainly on the differential shrinkage in tangential and radial direction but also that cupping is reduced to some extent by the creep of the surface layer. However during the conditioning treatment cupping increases to values near those reached after stress free drying. Although many methods of drying timber have been tried over the years only a few of these enable drying to be carried out at a reasonable cost and with minimal damage to the timber. The most common method of drying is to extract moisture in the form of water vapour. To do this, heat must be supplied to the wood to provide the latent heat of vaporisation. There are several ways of conveying heat to the wood and removing the evaporated moisture. Nearly all the world's timber is, in fact, dried in air. This can be carried out at ordinary atmospheric temperatures (air drying), or in a kiln at controlled temperatures raised artificially above atmospheric temperature but not usually above 100°C, the boiling point of water. Air drying and kiln drying are fundamentally the same process because, with both, air is the medium which conveys heat to the wood and carries away the evaporated moisture [4-6].

2. FACTORS INFLUENCING THE DRYING OF WOOD IN AIR

The factors which will be described are those which affect wood when dried in air (in the open or in a kiln). There are several other ways in which wood can be dried, in chemicals, in a vacuum etc. Under these conditions different factors come into play.

- Vapour Pressure and Relative Humidity
- Temperature:
- Air Movement:
- Movement of Moisture in the Wood :
- Supply of Heat:

3. METHODS OF DRYING WOOD IN AIR

Air Drying

With air drying there is virtually no control of the temperature, relative humidity or speed of the air passing through the timber stacks. The rate of drying is therefore dependent on all the vagaries of the local climate and can vary between practically zero on a calm, damp day to quite fast enough to cause surface checking during dry, windy weather. With air drying, wood cannot be dried below its equilibrium moisture content and this will vary depending on the atmospheric conditions. So, except in unusually hot and dry weather, the lowest moisture content obtainable is around 16-17%; air drying alone is not sufficient for timber intended for most interior uses in Europe, Japan or N. America where a moisture content of between 8 and 12% is required. In air conditioned buildings moisture contents of about 12% should be anticipated.

Kiln Drying

In contrast to air drying a modern conventional drying kiln provides temperature control and a steady and adequate flow of air over the timber surface. The air flow rate and direction is controlled by fans and the temperature and relative humidity of the air can be adjusted to suit the species and sizes of timber being dried. It is thus possible to make full use of the increase in drying rate which can be achieved by raising the temperature to the maximum value which a particular timber species can tolerate without excessive degrade. At the same time, the relative humidity can be controlled so that the moisture gradients in the wood are not steep enough to cause surface checking. The same principles apply to the use of heat pump kilns except these recover and re-use a proportion of the energy which in conventional kilns is lost during the drying process when the warm, damp air is vented. In addition to the advantages of more rapid drying and limitation of degrade, the ability to control drying conditions in a kiln means that it is possible to achieve timber moisture contents suitable for specific uses. The direct costs of kiln drying are much higher than those of air drying for they include the capital costs of the equipment and the cost of fuel, electricity and supervision. These costs are partially or wholly offset by the reduction in stock level [7-10].

Air Drying Followed by Kiln Drying

Kiln drying tends to become uneconomical when the species and size of timber being dried require long kilning times. Therefore, with material taking more than about 4 or 5 weeks to kiln dry from green it will often be more economical to air dry the timber to about 25-30% moisture content before completing the drying in a kiln. The economic advantage of this approach may be lost, however, if the layout or lack of handling facilities necessitates dismantling the air dried stack and repiling for the kiln drying phase. Also with some species, the amount of splitting and checking which occurs during air drying in the dry season can be excessive.

4. MOISTURE CONTENT OF TIMBER

The amount of water in a piece of wood is known as its moisture content. Because this is expressed as a percentage of the dry weight of the piece, not of the total weight, it is possible to have moisture contents of well over 100%. The moisture content of green wood varies greatly from one species to another. Moisture content can vary between apparently similar pieces of the same species and in addition there may be differences, between and within species, in the rates at which moisture is lost from timber during drying. These inherent differences in timber mean that it is important during the drying process to be able to monitor moisture content and check that the drying process is proceeding correctly.

Moisture Content Determination by the Oven Drying Method

The oven drying method is the standard way of determining wood moisture content. With this method a piece of wood is initially weighed and then dried in an oven at 103°C ± 2°C. Drying is continued until the piece is completely dry (when no further weight loss occurs) and this oven dry weight recorded. The loss in weight during drying indicates how much water was originally present in the piece and the moisture content can be calculated simply, as follows:

$$\text{Initial moisture content (\%)} = \frac{\text{Initial (wet) weight - Dry weight}}{\text{Dry weight}} \times 100$$

For example, if the initial weight of the piece was 30.51g and its dry weight 22.60g, then the difference of 7.91g is the weight of moisture initially in the piece and its initial moisture content would be:

(30.51 - 22.60)/22.60 x 100 = 7.91/22.60 x 100 = 35.0% Alternatively the formula can be written:

Moisture content (%) = [(Initial weight/Dry weight) - 1] x 100

So that only the division sum needs to be carried out:

[(30.51/22.60) - 1] x 100 = 0.35 x 100 = 35.0 %

5. EQUIPMENT REQUIRED

Oven drying requires a well ventilated oven which can control the temperature to between 101 and 105°C and a balance for weighing the test samples. The balance should have a capacity of about 200g and be capable of detecting differences of 0.005g, an automatic type is recommended as these give an instantaneous reading. Infrared ovens are available for rapid drying. In some of these the heating lamps are directed on to the test section on the pan of a balance (incorporated in the equipment). Drying takes from about 3 to 10 minutes according to species and moisture content. However only one piece can be dried at a time and experience is needed to avoid overheating which can cause inaccurate results [11].

6. THE PRE-DRYING OF TIMBER

A high proportion of the world's timber is either wholly or partly air dried before drying in a kiln. Air drying involves the open piling of fresh-sawn timber out of doors, or in open sheds, so that the wood surfaces are exposed to the surrounding atmosphere. Wind and local convection currents will cause air movement through the stack and this conveys solar heat energy to the wood and carries away evaporated moisture[12]

The employment of correct techniques can reduce air drying times and keep drying degrade to a minimum.

Sitting and Layout of Yard

Ideally, timber should be stacked well away from trees and buildings on a cleared, level and well drained site which has been concreted, covered with ashes or treated to prevent the regrowth of vegetation [13]. In most situations, the orientation of the stacks has little effect on the drying rate and the most important consideration in planning the yard is to arrange stocks and roadways to facilitate handling. Adjacent stacks should be parallel and oriented with either ends or sides to the roadway depending on the methods used for transport and stacking. Consideration should be given to the possibility of fork-lift trucks or side loaders. Stacks should be erected on good solid foundations and, in order to permit ample ventilation, the bottom layers of timber should be raised well above the ground. The clearance should certainly be no less than 230mm and should preferably be about 460mm. The most convenient form of foundation, and probably the simplest to erect, consists of a series of timber cross-members (bearers) not less than 100 x 100mm in section, preferably preservative-treated and lifted clear of the ground on brick or concrete piers or on treated timber, e.g. railway sleepers (figure 1). The piers should be placed at intervals of 600mm along the whole length of the stack. Stringers or longitudinal timber members can be used to give added strength and rigidity to the foundations, but they are generally only necessary where special stacking arrangements are involved. It is essential that the bearers should all be in one plane, but it is not critical whether these are level or on a slight slope [14]. In either case, any necessary adjustment can be made by varying the height of the brick piers and inserting wooden packing blocks between the bricks and cross-members where required.

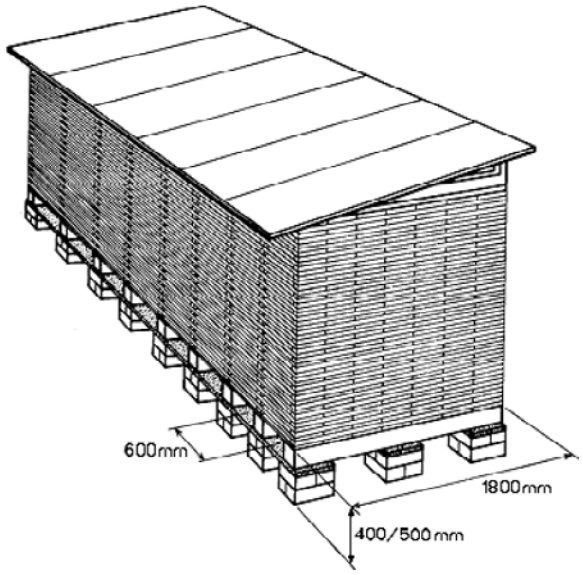

Figure 1. Recommended stack construction for air seasoning of timber.

The Normal Method of Stacking

Whenever possible, different species and thicknesses should be stacked separately. It is an advantage if timber can be sorted to length at the outset, and when a variety of lengths has to be stacked it is convenient to place the longest pieces at the bottom and to reduce the length of the stack as the height increases [15]. Alternatively, if sorting beforehand is not practicable, a stack of uniform length may be built by arranging the timber as shown in figure 2. This is sometimes referred to as box-piling.

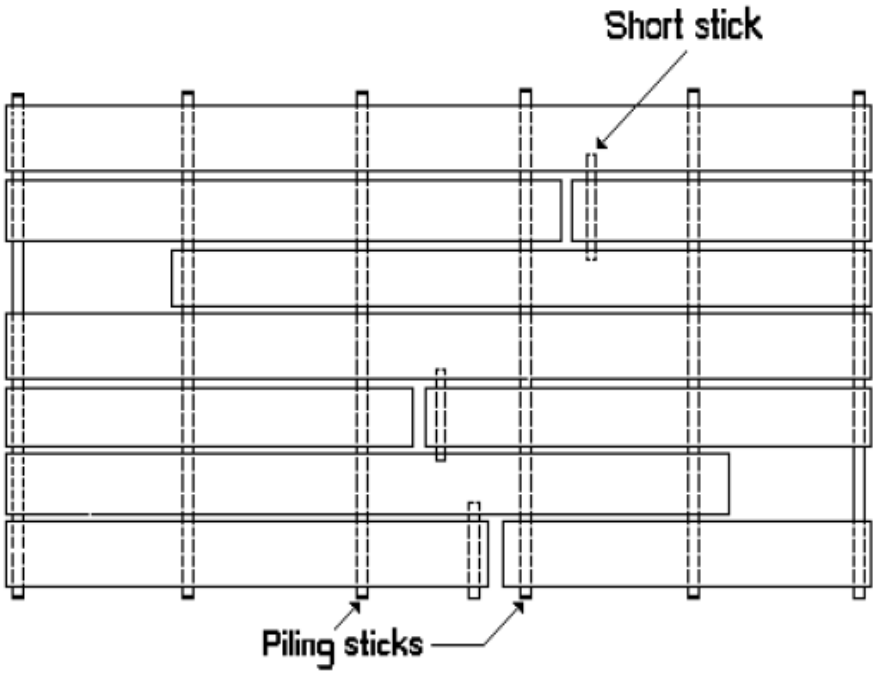

Figure 2. Plan view of layer of boards.

7. KILN DESIGN

In two designs of overhead fan kiln the fans are mounted at regular intervals on a longitudinal drive shaft. The air is diverted by baffle boxes to flow across the top of the kiln above a false ceiling, down the side and through the load as in the designs shown below (figure 3) sometimes called cross circulation kilns. In design A, in spite of correcting plate baffles fixed as indicated, there is a tendency for the circulation to be stronger at the end towards which the fans are blowing. This effect is eliminated in design B in which left and right hand fans are fitted alternately on the shaft, although here a slight loss in efficiency of the fans will occur because opposing pairs will set up back pressure [16-18].

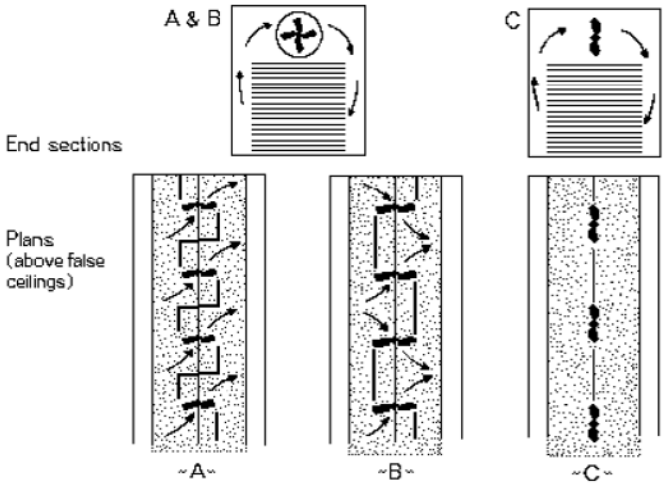

Figure 3. Fan arrangements in three designs of overhead fan kiln.

In these longitudinal shaft kilns, air speeds through the load average only from 0.5 to 1 m/s, unless fans larger than the usual 0.8 to 1.Om diameter are used. In America kilns are built to design B using fans up to 1.8m in diameter. There are two distinctive types of side fan kiln - the vertical flow (figure 4) and the horizontal flow (figure 4, design E). In both, large propeller type fans are placed to one side of the timber load. With side fan designs it is possible to take advantage of the greater energy efficiency of the slower running, larger fans without the need for increased kiln height which would be necessary if these were used in an overhead fan design. In design D1 the air is delivered or returned through a duct which passes air above the timber load and no transverse baffles are required [19-21]. In a variation of this design (D2) smaller fans are mounted to one side of the lower half of the timber load and the air return not through a duct but through the upper half of the load.

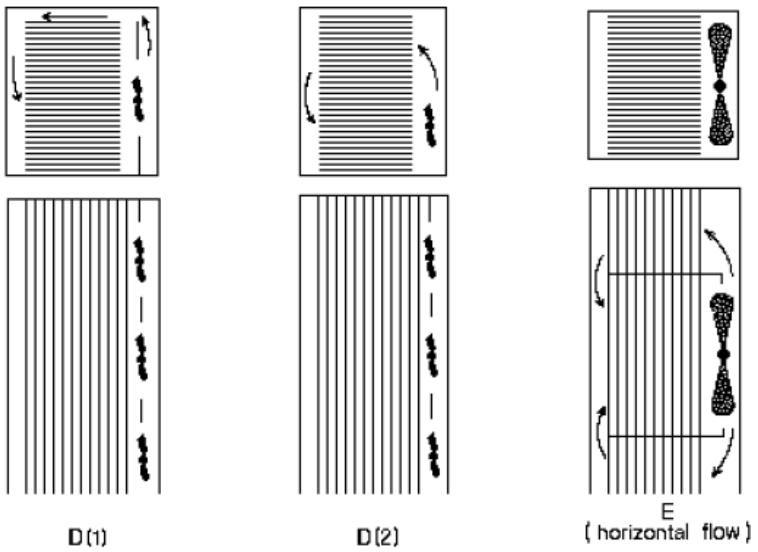

Figure 4. Fan arrangements in three designs of side fan kiln.

In design E, which is a type commonly installed in the UK and in some European countries, the air flow is horizontal throughout. This is achieved by filling the kiln to its full height and, with the wing baffles forming a fan box, air is pulled or pushed (according to the direction of fan rotation) through the portion of the load opposite the fan and pushed or pulled through the two end portions. In designs D2 and E, the air has to pass through the load twice before it is reheated (unless booster heating is placed in a position remote from the fans) and fast air speeds are necessary to minimize the difference in drying rate across the width. Average speeds of the order of 1.5 to 2.4m/s are obtained without excessive power consumption by the use of large fans 1.4-2.4m in diameter. The air speeds through various parts of the timber load are not usually as uniform as in the overhead cross shaft type of kiln but the lowest speed within the load is sufficient for satisfactory drying [18-20]. It is now normal to reverse the direction of air flow frequently and this compensates for local variations in air speed. Side fan kilns can also be built as double load units, the one large fan pulling air through the load on one side of it and pushing the air through that on the other. The traditional and simplest instrument for measuring air conditions is the wet and dry bulb hygrometer (figure 5). The dry bulb thermometer measures the actual temperature in the kiln while the wet bulb reading enables the relative humidity of the air to be estimated. The bulb of the wet bulb thermometer is surrounded by a sleeve which is kept moist with distilled water from a reservoir. Evaporation from this sleeve cools the wet bulb below the temperature of the dry bulb and the magnitude of this wet bulb depression is related to the relative humidity of the air.

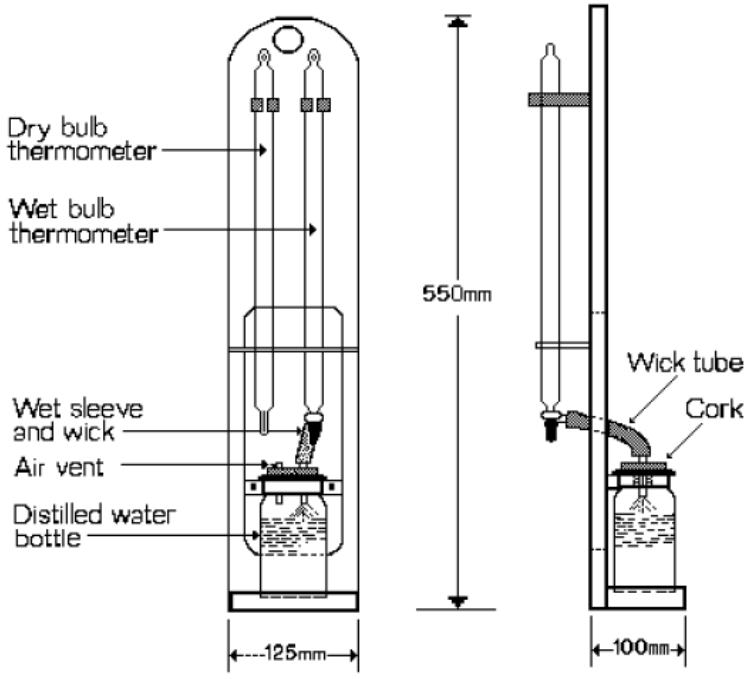

Figure 5. Wet and dry-bulb hygrometer.

Microprocessor and computer technology has already assumed a major role in the development of control systems for kiln drying. Most computer based systems can be

programmed to operate the kiln according to a predetermined schedule, while more advanced systems are able to control a sequence of kiln conditions on the basis of the moisture content of the timber, which is monitored by remote sensors in the load. There is still technical difficulty in measuring accurately moisture contents above about 30% and at present fully automatic control systems require a greater margin of safety above this level and consequently drying times may be slightly longer [20-22].

In all types of kiln in which the circulating air returns in a vertical direction to the inlet, the sides of the load should be made as even as possible. Pieces which jut out appreciably will tend to act as deflectors causing an excess of air to pass through one or two spaces at the expense of others (figure 6). An advantage of the side fan kilns with horizontal air flow is that an irregular-faced load has no adverse effect on the circulation.

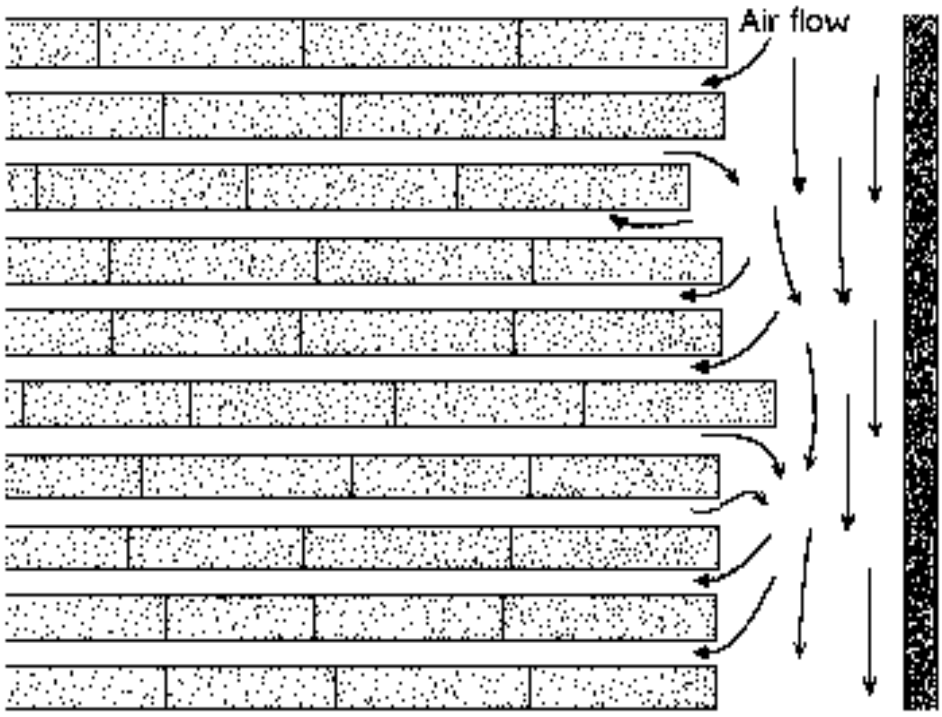

Figure 6. Effect of irregular pile face on air circulation.

Two other points should be noted in the piling of loads for horizontal flow kilns. The gaps between the face of the load and the end wings of the fan boxes should be as small as possible or should be blanked off to prevent excessive short-circuiting. Secondly, the sticks should be arranged so that there is a vertical tier opposite each end wing to ensure that air entering the load traverses the full width before re-entering and being pulled back into the fan (figure 7). Figures 8B and 8C show how incorrect piling can adversely affect the air circulation.

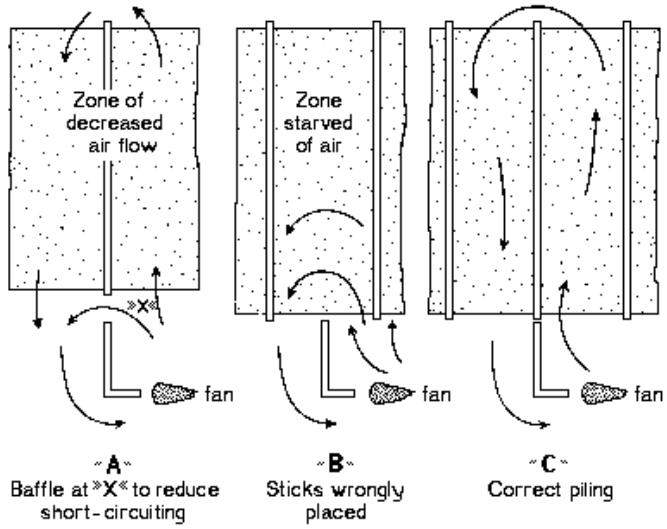

Figure 7. Piling of timber in side fan horizontal flow kilns.

In any kiln the circulating air will always have a tendency to by-pass the timber through spaces inadvertently formed above, below or along the load. It is recommended that this short-circuiting should be minimized by using canvas curtains or baffles made of wood or other suitable material. Occasionally the volume of timber to be dried may be less than a full load for the kiln available. In such cases the width of the load can be reduced so that it approximately fills the height of the kiln.

Certain timber items cut to standard sizes can conveniently be piled without the use of a large number of sticks. For instance, small furniture parts such as chair leg squares can be self crossed (figure 8). Here the individual pieces are so small that they can be used in place of the normal piling sticks without fear of restricting the air flow[23-25]. In order that the individual stacks which make up a complete load should be stable when drying shrinkage occurs, sticks should be introduced at intervals across the full width of the load.

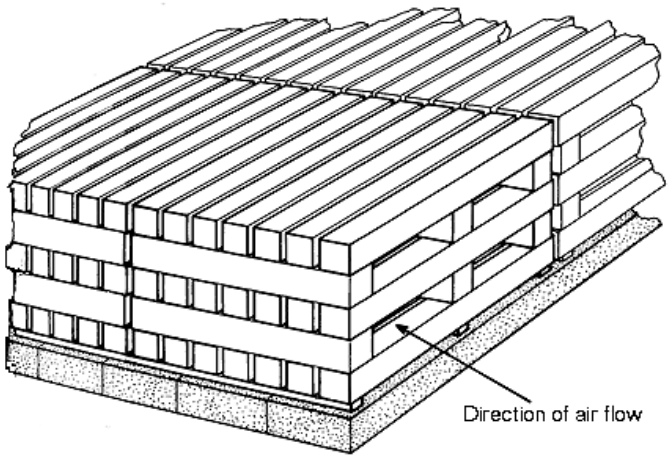

Figure 8. Cross-piling of dimension stock.

For a typical drying operation involving an average size kiln load, and a single species of timber converted through and through to a constant width, it is recommended that the number of sample pieces in the sample series (figure 9) is a minimum of six. This sample series should consist of both plain-sawn and quarter-sawn samples and if possible it should include pieces which are representative of the wettest and driest wood in the kiln load. The number of samples should be increased proportionately in larger kiln loads. However there is a practical and economic limit which may restrict the number that can be monitored [26-28]. For example in large loads containing more than one species of more than one thickness, it may be impractical to have enough samples to provide all the necessary information about the progress of drying. Conversely it may be possible to include less than six samples when kilning timber which has fairly uniform moisture content, and well known and predictable drying characteristics.

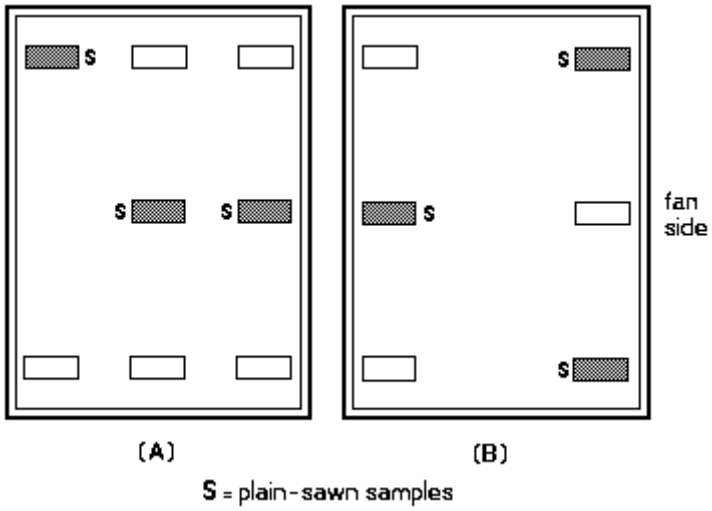

Figure 9. Distribution of samples in the load in a kiln (A) with overhead fans (B) with side fans and horizontal flow.

To ensure that the drying response of a sample is typical of the wood in a particular part of the load, samples must be incorporated in a way which does not interfere with local drying conditions. Additionally the method of incorporation must allow easy withdrawal of the sample for weighing. However difficulties of sample withdrawal may sometimes be unavoidable with timber which is prone to distort badly. One method of accommodating withdrawable samples is to place sticks over them which have been notched out to about half the normal thickness. This tends to be time consuming and rather wasteful of sticks unless it is feasible to have samples of a standard width and position, in which case the notched sticks can be used repeatedly. An alternative arrangement, using suitable lengths of sticks of half the normal thickness, is shown in figure 10. Both these methods involve opening the main kiln doors for the removal of the samples but with modern kilns the air conditions soon return to normal [29].

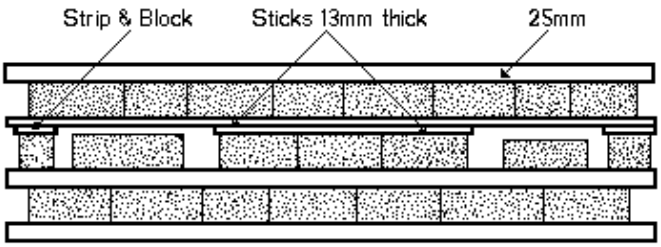

Figure 10. Method of accommodating withdrawable kiln samples.

Samples can be accommodated in the sides of loads by cutting one or more sticks off short (figure 11) leaving the sample free. Access to side samples is usually by the small side doors rather than by the main door and because the operator therefore has to enter the kiln, there may be practical difficulties in retrieving samples under certain kiln conditions.

Samples should always be positioned within the load and not mounted on short projections at the ends of loads, or between two separate loads, where abnormally fast drying may occur.

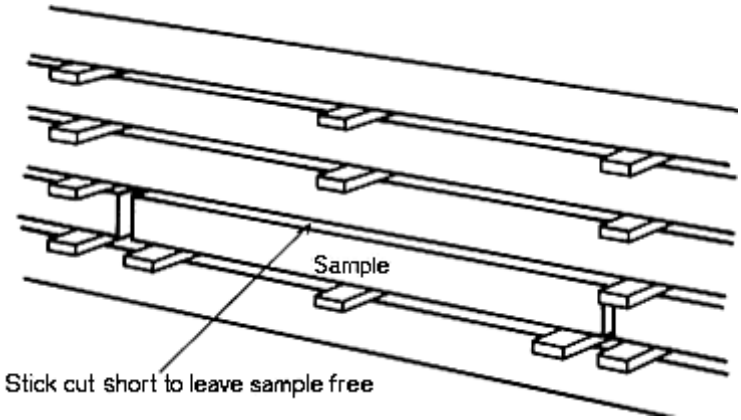

Figure 11. Method of accommodating sample in the side of a kiln stack.

As it is shown, for the duct formed by the boards the aspect ratio, AR, is very low in practice with

$$AR = (\text{duct height})/(\text{duct width}) < 0.1 \quad (1)$$

As duct height is considerably smaller than the duct width, it is assumed that the hydraulic diameter d_h asymptotically approaches twice the duct height (as is in the case of an infinity wide duct), i.e.

$$d_h = (2)\ (\text{duct height}) \quad (2)$$

This is a good approximation in most cases, but should be verified at higher aspect ratio.

The pressure loss of fully developed flow along a channel can be determined by using Moody chart [30] or a friction factor formula as described by White [31]. The dimensionless friction factor formula determined by Haaland [32] represents the turbulent region on the Moody chart and is as follows:

$$f_D^{-1/2} = -1.8\log_{10}\left(\frac{6.9}{\mathrm{Re}_{umd_h}} + \left(\frac{\sigma/d_h}{3.7}\right)^{1.11}\right) \tag{3}$$

The Reynolds number Re_{umd_h} is based on the average speed u_m and hydraulic diameter d_h, i.e.

$$\mathrm{Re}_{umd_h} = \frac{\rho u_m d_h}{\nu} \tag{4}$$

8. Estimation of the Average Moisture Content of a Sample

By first estimating and then monitoring the fall in average moisture content of the samples during drying, a given schedule can be followed accurately. The average moisture content for a particular sample is estimated by first measuring, using the oven method the moisture content of one (or more) test sections cut as indicated above. If it is then assumed that this measured moisture content is typical of the remainder of the sample, the dry weight of this remainder can be estimated and changes in its average moisture content can be monitored throughout drying by weighing. Suppose that the initial average moisture content of the sample was estimated to be 35%. If the sample weighed 12.40kg then its dry weight can be estimated:

Dry weight = (wet weight/moisture content)/100 + 1
=12.40/[(35/100) + 1]
=12.40/1.35
=9.18kg

This estimated dry weight remains a constant quantity as long as no further wood is cut from the sample. If after a period of drying the actual weight of the sample has fallen to 11.72kg, its new average moisture content can be estimated as follows:

New average moisture content = [(Current weight/Dry weight) - 1] x 100
=[(11.72/9.18) - 1] x 100
=27.6%

This technique is based on the assumption that the test section(s) do provide an accurate estimate of the average moisture content of the sample from which they were cut. However, even in the ideal situation where a section is removed from each end of the sample (and the values obtained averaged) an appreciable error can occur. This is because moisture content will inevitably vary along the length of a piece and for this reason it is always advisable to predetermine the moisture content of a further batch of test sections towards the end of a kiln run [30]. With certain species, such as teak, there is a marked tendency to retain pockets of moisture along the length. In these cases the average moisture content is difficult to determine in the normal way and, if it is necessary to dry such timbers to uniform moisture content, there will be a need to cut more test sections to obtain a suitably accurate estimate of average moisture content.

9. Estimation of the Average Moisture Content of the Load

Having obtained the average moisture contents for the individual samples, it is then quite straight-forward to use this information to estimate the average moisture content of the load. Again, this can be estimated at any time during drying and it helps the kiln operator to judge the progress of drying. It is estimated simply, as follows:

$$\text{Average moisture content of the load} = \frac{\text{Sum of average moisture contents for all for all samples being used to monitor the load}}{\text{Total number of samples being used to monitor the load}}$$

For example, if at a particular time, the samples gave average moisture contents of 16, 14, 13, 12, 10 and 10%: Average moisture content of the load

= (16+ 14+ 13+ 12+ 10+ 10)/6
= 75/6
=12.5%

Once below fiber saturation point, electrical resistance moisture meters can be used to augment the information obtained by oven drying.

10. Assessment of Moisture Distribution and Casehardening Stresses

The importance of assessments of moisture distribution and casehardening is in evaluating the risk of drying degrades. Both assessments can only be made by cutting fresh test sections. It is often convenient to cut these at the same time as sections are taken for the average moisture distribution. Casehardening stresses should be assessed at least twice during a kiln run: first before drying is commenced (to ensure that the appropriate drying schedule

will be suitable without modification) and again towards the end of the kiln run to ensure that drying is progressing correctly. More assessments may be necessary when drying difficult sizes of timber or species which have unpredictable drying qualities. Moisture distribution is assessed by removal of a test section and by sub-dividing this into strips as shown in figure 12. The strips are cut so that the inner and intermediate strips are representative of increasing depth within the original sample. Moisture distribution is then assessed by measuring by moisture content of each strip separately by the oven method. In parallel (figure 12) a section can be removed for casehardening tests. Although these assessments are time-consuming and labor intensive, careful monitoring in the manner indicated will always be economic if it avoids extensive and unnecessary degrade within a load [32].

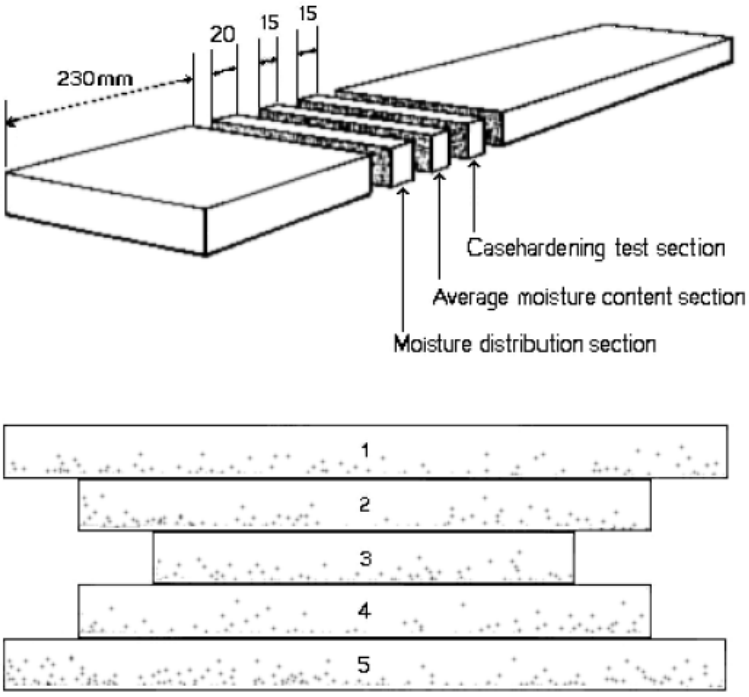

Figure 12. Re-cutting of kiln sample for testing moisture content, average and distribution: also casehardening.

11. MOISTURE TRANSFER ANALYSIS

During drying transient heat transfer takes place and therefore the Biot number provides a measure of the temperature drop in the solid relative to the temperature difference between the surface and the fluid and hence shows the internal external (surface) resistances to the heat transfer from or to object [33].

$$Bi = kL / D \tag{5}$$

$$F_O = Dt / L^2 \tag{6}$$

The Fourier number is considered as $F_O = (\alpha t)/(L^2)$ where α is the thermal diffusivity, $m^2 s^{-1}$; and t is the process time, s.

The one dimensional transient moisture diffusion equation can be written as:

$$D\left(\partial^2 W / \partial z^2\right) = \left(\partial W / \partial t\right) \text{ and } D\left(\partial^2 \phi / \partial z^2\right) = \left(\partial \phi / \partial t\right) \tag{7}$$

Equation (7) is subjected to the following initial and boundary conditions:

$$\phi(z,0) = \phi_i = \left(W_i - W_e\right)$$

for $0.1 \prec Bi \prec 100$ and $Bi \succ 100$ (8)

$$\left(\partial \phi(0,t) / \partial z\right) = 0$$

for $0.1 \prec Bi \prec 100$ and $Bi \succ 100$ (9)

$$-D\left(\partial \phi(L,t) / \partial z\right) = k\phi(L,t)$$

for $0.1 \prec Bi \prec 100$; $\phi(L,t) = 0$

for $Bi \succ 100$ (10)

where $\phi = \left(W - W_e\right)$

and the moisture content at a point of the solid object is non-dimensionalized by the following equation:

$$\Phi = \left(W - W_e\right)/\left(W_i - W_e\right) \tag{11}$$

Solution to the governing equation (i.e. Eq.(7)) under the corresponding boundry condition with $\Gamma = 0 / z = 0$, yield dimensionless average moisture distribution of the corresponding slab objects in the following form [33] :

$$\Phi = \sum_{n=1}^{\infty} A_n B_n \text{ for } 0.1 \prec Bi \prec 100 \text{ and } Bi \succ 100 \tag{12}$$

where

$$A_n = \left(2 \sin \mu_n\right)/\left((\mu_n) + (\sin \mu_n \cos \mu_n)\right)$$

for $0.1 \prec Bi \prec 100$ (13)

$$A_n = \left(2(-1)^{n+1}\right)/(\mu_n) \qquad \text{for } B_i \succ 100 \tag{14}$$

$$B_n = \exp\left(-\mu_n^2 F_O\right) \qquad \text{for } 0.1 \prec Bi \prec 100 \text{ and } B_i \succ 100 \tag{15}$$

Further simplifications can be made in Eq. (12) by taking $\left(\mu_1^2 F_O\right) \succ 1.2$. Thus, the infinite sum in Eq. (12) is well approximated by the first term only, i.e.[33],

$$\Phi = A_1 B_1 \tag{16}$$

where $\left(2\sin\mu_1\right)/\left((\mu_1) + (\sin\mu_1 \cos\mu_1)\right)$

for $0.1 \prec Bi \prec 100$ (17)

$$A_1 = \left(2/\mu_1\right) \text{ for } B_i \succ 100 \tag{18}$$

$$B_1 = \exp\left(-\mu_1^2 F_O\right) \text{ for } 0.1 \prec Bi \prec 100 \text{ and } B_i \succ 100 \tag{19}$$

12. EXPERIMENTAL

Fifty cylindrical green wood samples of Spruce were obtained from Guilan province. The diameter and height of the specimens were approximately 300mm and 21mm respectively. A programmable domestic microwave oven (Deawoo,KOC-1B4K), with a maximum power output of 1000 W at 2450 MHz was used. The oven has the facility to adjust power (Wattage) supply and the time of processing. The hot air drying experiments were performed in a pilot tray dryer consisted a temperature controller. Air was drawn into the duct through a mesh guard by a motor driven axial flow fan impeller whose speed can be controlled in the duct. The infrared dryer was equipped with eight red glass lamps (Philips) with power 175 W, each emitting radiation with peak wavelength 1200 nm. Radiators were arranged in three rows, with three lamps in each row. Dryer was equipped with measuring devices, which made it possible to control air parameters. The amount of water in a piece of wood is known as its moisture content. All the 50 dried samples were tested on a universal Tension Test machine model (Hounsfield HS100KS), with a loading capacity of 100 KN. During the tensile testing, the stress-strain curves as well as the peak load were recorded.

13. RESULTS

Conventional hot air drying is one of the most frequently used operations. The drying curves for conventional hot air drying of wood samples are shown in figures 13-18. It can be observed that the drying usually take place in the falling rate period. In essence, air in the oven is saturated, by time, and forms a thick film around the wood sample. That prevents effective separation of the evaporated moisture from the wood. This may be the reason for existence of constant rate period in this study.

Microwave drying is an alternative drying method, which is recently used in different industries. The effect of changing power output in the microwave oven on the moisture

content is shown in the figures 18-22. At all power levels, drying curves were tended to end at about the same time. The observed initial acceleration of drying may be caused by allowing rapid evaporation and transport of water.

Infrared radiation is transmitted through water at short wavelength, it is absorbed on the surface. Infrared radiation has some advantages over convective heating. Heat transfer coefficients are high, the process time is short and the cost of energy is low. In this study, the drying time was reduced by nearly 34% compare to hot air drying. The drying curves were plotted in figures 23 and 24. In contrast to the hot air drying curves which had a short constant rate period followed by a falling rate period, figures 23 and 24 indicates that the infrared had only a falling rate period.

All dried samples were tested on a Hounsfield universal tension test machine with a loading capacity of 100 KN (figure 25). . The results of tensile loading of dried samples are presented in figures 26-29. It is clear that the microwave dried spruce specimen with failure strength of 49.6 Mpa has made a significant property improvement (figure 26). The normal stiffness of infrared dried sample is reported as 35.0 Mpa (figure 27) whereas the oven dried sample showed strength of about 44.5 Mpa (figure 28). From figure 29 it is revealed that the natural convection dried specimens are the strongest (50 Mpa). In practice the drying time for this can take up months and years. In figure 30 the strength of dried samples are compared for a better judgment.

14. INDUSTRIAL APPLICATION OF THE RESULTS

In wood drying process we should note that the wood can hold moisture in the cell lumen (cavity) as liquid or "free" water, or as adsorbed or "bound" water attached to the cellulose molecules in the cell wall. Meanwhile, the occurrence of the free water does not affect the properties of wood other than its weight. Bound water, however, does affect many properties of wood, and is more difficult to remove in the drying process. Microscopically, the dimensional change with MC is anisotropic (referring to the fact that wood has very different properties parallel to the fact grain versus the transverse direction). As the MC decreases, wood shrinks; conversely, as the MC increases, wood swells or grows larger. The process of drying focuses on producing wood with an MC about the same as the equilibrium value for the intended service environment.

For the design of dryers it is necessary to carry out drying experiments at various drying conditions. Experimentally determined drying times, transition points, and constant-rate regime temperature can then be used as a base case for the analytical results. Based on the information from the experimental trials, runs with lower amounts of moisture to evaporate, higher dryer temperatures, should be expected to dry faster and reach transition point more rapidly. After an initial increase or decrease of the rate of drying, the drying process enters the constant rate period. This initial change of the rate of drying is caused by a variation of the surface temperature which in turn results in a change of vapour density.

It can be noted that time interval of drying process is solely determined by external conditions. Once the drying process has entered the falling rate period, the external conditions become relatively unimportant compared to the internal parameters.

By comparing runs with the same initial moisture, we see that as oven temperature increases, the transition points are reached more quickly and total drying times are shorter. Sample temperatures are higher because they are exposed to higher heat transfer rates, giving rise to higher mass transfer rates during the constant-rate regime.

The experimental study suggests that the humidity of the free stream should be as low as possible. Partial recirculation, 100% fresh air intake, or dehumidifications are some of the possible ways to accomplish this task, but a cost analysis is imperative before deciding on any option.

Reduction of the drying time in microwave heater seems to be a motivating cost saving factor for industries. In this case a moderate mechanical property is obtained (table 1). To minimize directional variations in use, wood needs to be dry enough to match the service environment.

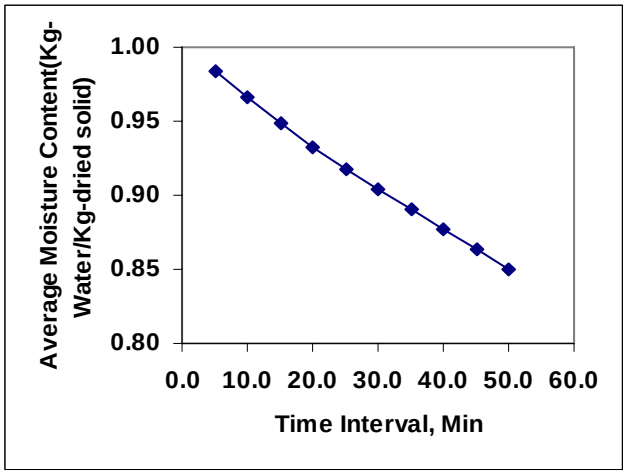

Figure 13. Average moisture content versus time; (Conventional hot air-dried wood at T= 40°C).

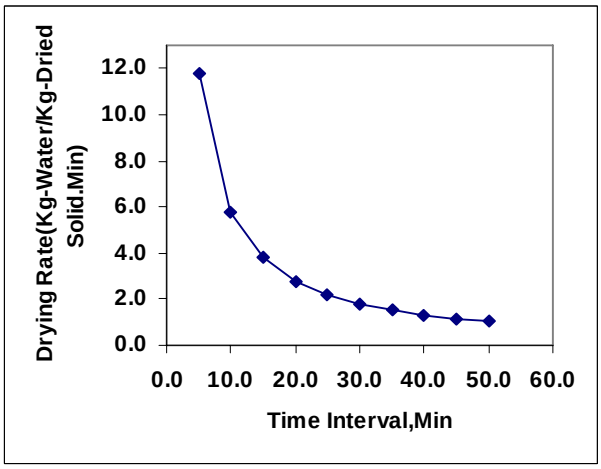

Figure 14. Drying rate curve; (Conventional hot air-dried wood at T=40°C).

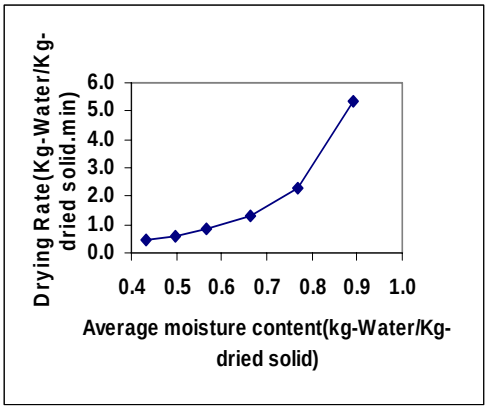

Figure 15. Average moisture content versus time; (Conventional hot air-dried wood at T=100°C).

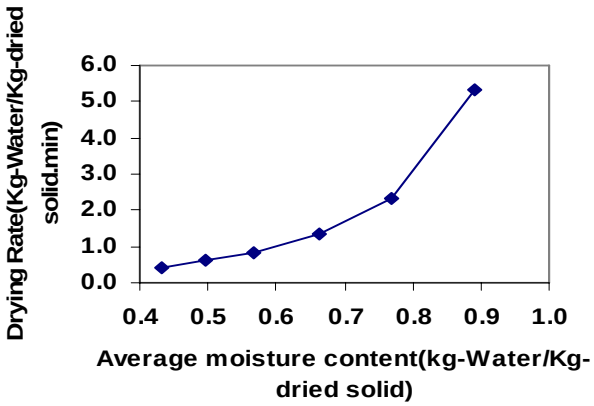

Figure 16. Drying rate curve; (Conventional hot air-dried wood at T=100°C).

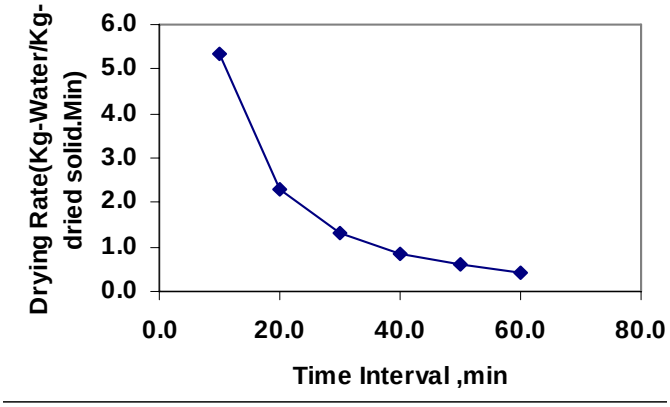

Figure 17. Drying rate curve; (Conventional hot air-dried wood at T=100°C).

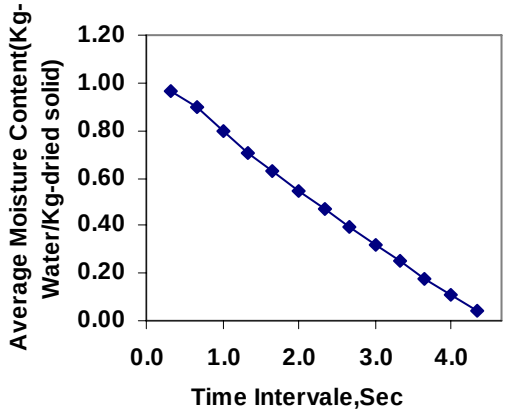

Figure 18. Drying curve for microwave-dried wood at 80powers.

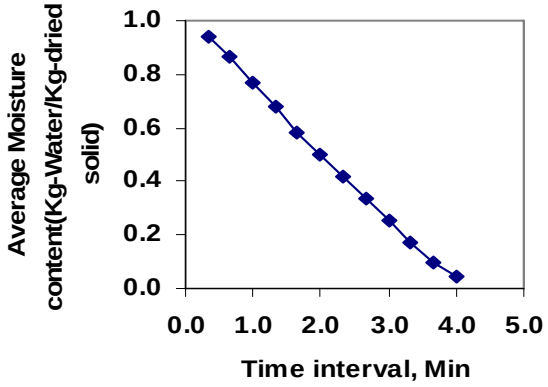

Figure 19. Drying curve for microwave-dried wood at 100% powers.

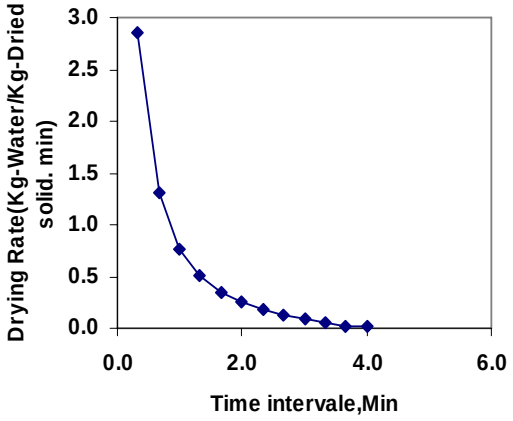

Figure 20. Drying rate curve for microwave-dried wood at 100% power.

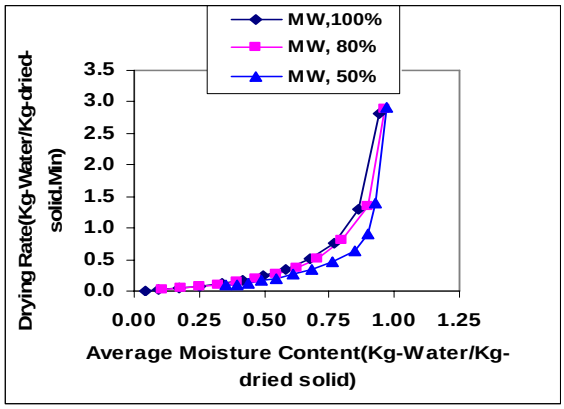

Figure 21. Drying rate curves for microwave-dried wood at three different power.

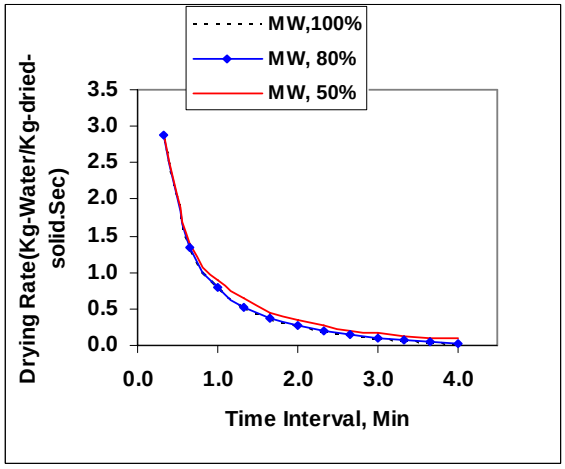

Figure 22. Drying rate curves for microwave-dried wood at three different powers.

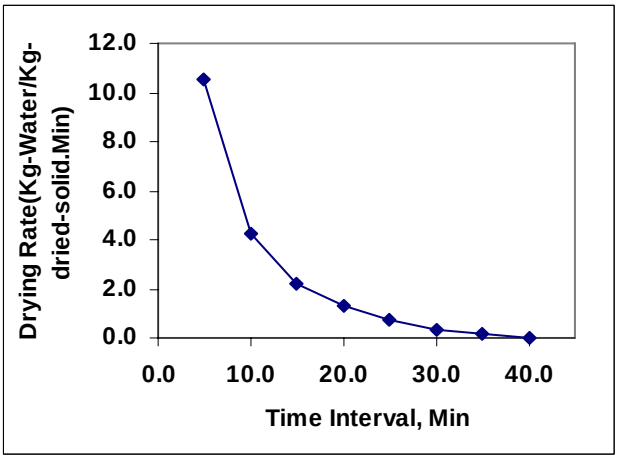

Figure 23. Drying curve for infrared-dried wood at 100% powers.

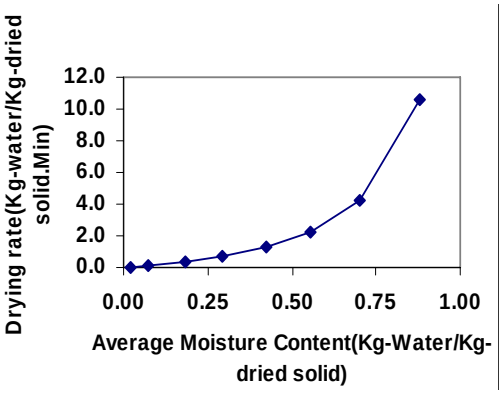

Figure 24. Drying curve for infrared-dried wood at 100% powers.

Figure 25. Tension test.

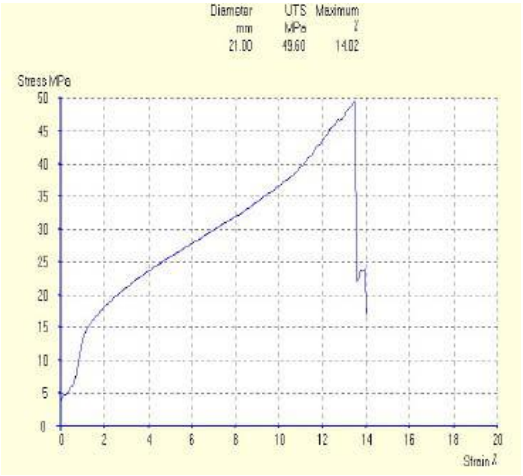

Figure 26. Stress-strain for microwave dried wood.

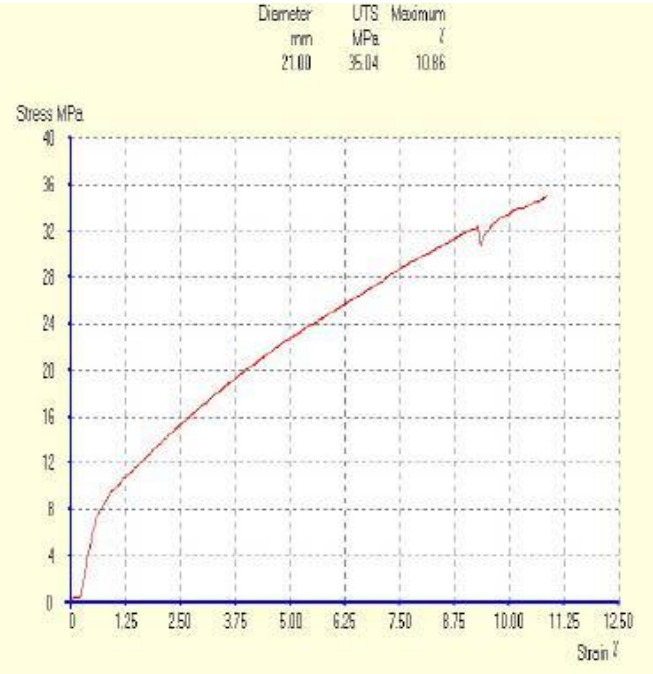

Figure 27. Stress-strain for infrared dried wood.

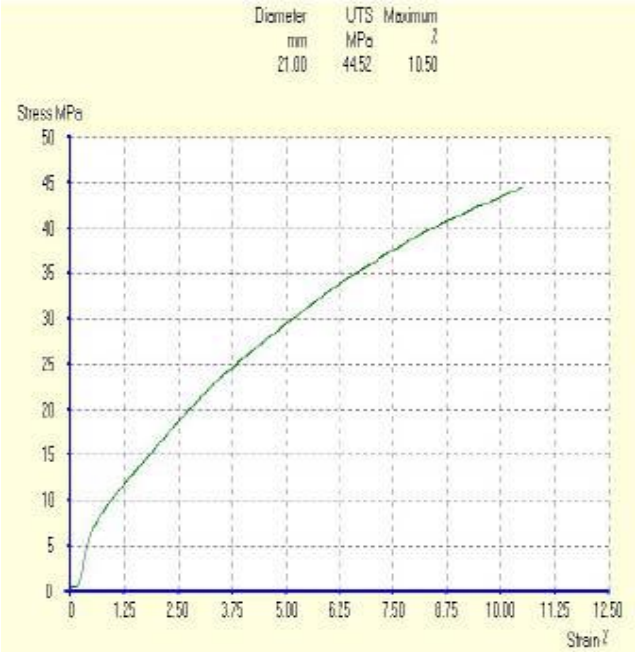

Figure 28. Stress-strain for hot-air dried wood.

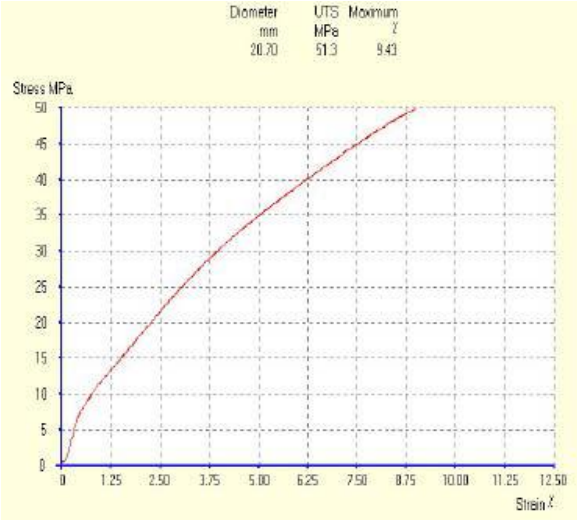

Figure 29. Stress-strain for natural convection dried wood.

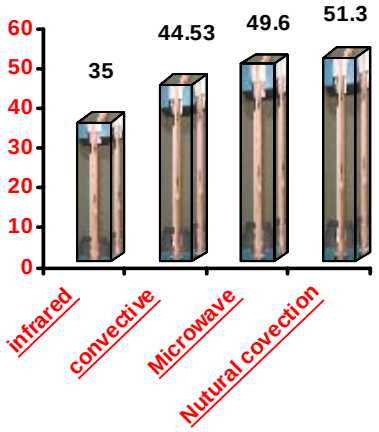

Figure 30. Strength of dried wood samples in three different.

Table 1. Average strength properties of samples (σ values in brackets refer to standard deviations

Drying Method	Failure Strength(Mpa)	Failure Strain %	Yield Strength(Mpa)	Modulus of elasticity(Gpa)
Natural convection Dried wood	51. 3 (σ2.44)	9. 43	12. 8 (σ 0. 615)	0. 544 (σ 0. 058)
Hot air dried wood	44. 53 (σ 1.72)	10. 5	13. 3 (σ 0. 51)	0. 424 (σ 0. 05)
Infrared dried wood	35. 04 (σ 1.16)	10. 86	10. 5 σ (0. 35)	0. 322 (σ 0. 035)
Microwave dried wood	49. 6(σ 4. 51)	14. 02	17. 0 (σ 1. 28)	0. 354 (σ0. 054)

CONCLUDING REMARKS

Convective drying of wood is an old technology, and yet is an immature method. A comprehensive as well as state-of-art review on wood drying process has been made in this paper. Many challenges exist in wood drying process, and a number of fundamental questions remain open. Because of limitations as summarized in this paper, most are considered as perspective in the future. Microwave heating and drying of wood products has not been used to a larger extent by the wood industries and manufactures. This could be explained by the insufficient knowledge of the complex interaction between material and process parameters during heating and drying as well as by the required investment expenses. The knowledge and understanding of the process will be improved as well as applying this technique in the most effective way. Its benefit is the fast drying rate.

Although many methods of drying timber have been tried over the years only a few of these enable drying to be carried out at a reasonable cost and with minimal damage to the timber. The most common method of drying is to extract moisture in the form of water vapor. To do this, heat must be supplied to the wood to provide the latent heat of vaporization. The temperature of a piece of wood and of the air surrounding it will also affect the rate of water evaporation from the wood surface. With kiln drying, warm or hot air is passed over the timber and at the start of the drying process the temperature differential between the air and the wet wood will usually be large. As a result, heat energy will be transferred from the air to the wood surface where it will raise the temperature of both the wood and the water it contains. Water, in the form of vapor, will then be lost from the wood surfaces, provided the surrounding air is not already saturated with moisture. This results in the development of a moisture content gradient from the inside to the outside of the wood. As the temperature is raised this increases not only the steepness of this moisture gradient, but also the rate of moisture movement along the gradient and the rate of loss of water vapor from the surface of the wood. At a given temperature the rate of evaporation is dependent on the vapor pressure difference between the air close to the wood and that of the more mobile air above this zone.

Unfortunately the considerable benefits obtainable by raising the drying temperature cannot always be fully exploited because there are limits to the drying rates which various wood species will tolerate without degrade. In the drying of many species, especially medium density and heavy hardwoods, shrinkage and accompanying distortion may increase as the temperature is raised. So with species which are prone to distort it is normal to use comparatively low kiln temperatures. In contrast to hot air drying a modern radiation drying provides temperature control and a steady and adequate flow of air over the timber surface. The air flow rate and direction is controlled by fans and the temperature and relative humidity of the air can be adjusted to suit the species and sizes of timber being dried. It is thus possible to make full use of the increase in drying rate which can be achieved by raising the temperature to the maximum value which a particular timber species can tolerate without excessive degrade.

REFERENCES

[1] Scheigger, A. E., "The physics of flow through porous media, University of Toronto Press" 1958.

[2] Plumb, O. A.,and Spolek, G. A., and Olmstead, B. A., "Heat and Mass Transfer in wood drying" *Int. J. Heat Mass Transfer*,Vol. 28, 1985,pp. 1669-1678

[3] Basilico, C., and Martin, M., "Approache expèrimentale des mecanismes de transfert au cours du séchage convective à haute temperature d'un bois"(In French), *Int. J. heat Mass Transfer*,*Vol*. 27, 1984 ,pp.657-688

[4] Jackson, G. and James, D., The permeability of fibrous porous media, *Can. J. Chem. Eng*. 64, pp. 207-221, 1986.

[5] Hunter, A. , On the basic equation of sorption and isosteric heat, *Wood Sci. Technol*. 25, pp 99-111, 1991.

[6] Hunter, A. On the movement of water through wood-the diffusion coefficient, *Wood Sci. Technol.* 27, pp 401-408, 1993.

[7] Hunter, A., A Complete theoretical isotherm for for wood, based on capillary condensation, *Wood Sci. Technol.* 30, pp. 127-131, 1996.

[8] Hudson, M., Improved method of an apparatus for dehydrating wood and wood products, US Patent No 655062

[9] Kifetew G., Thuvander, F. and Berglund, L., The effect of drying on wood fracture surfaces from specimens loaded in wet condition, *Wood Sci. Tecnol.* 32, pp 83-94, 1998.

[10] Thuvande, F. and Berglund, L., A multiple fracture test for strain to failure distribution in wood, *Wood Sci. Technol.* 32, pp. 227-235, 1998.

[11] Bousquet, D., Drying wood, University of Vermont Extension Brieflet 1326, 1998.

[12] Cech, M. and Pfaff, F., Kiln Operator's Manual for Eastern Canada, Forintek Canada Corp. Eastern Forest Products Laboratory, Ottawa, Canada, 2004.

[13] Culpepper, L., High temperature drying-enhancing kiln operations, Miller Freeman Publications, Inc., San Francisco, 1990.

[14] Hart, C., Kiln overheating when conditioning Lumber, *Forest Prod. J.,* 40, pp. 9-14, 1990.

[15] Kayihan, F., Simultaneous heat and mass transfer with local three-phase equilibra in wood drying, Proc. 3rd International Drying Symposium, 1, pp. 123-134, 1982.

[16] Kelsey, K. and Clarke, L., The heat of sorption of water by wood, Australian *J. Appl. Sci.* 7, pp. 160-175, 1965.

[17] Pang, S., Moisture content gradient in a softwood board during drying, *Wood Sci .Technol.* 30, pp. 165-178, 1996.

[18] Pang, S., External heat and mass transfer coefficients for kiln dring of timber, *Drying Technol.* 14, pp. 859-871, 1996.

[19] Pang, S. Some considerations in simulation of superheated steam drying of softwood lumber, *Drying Technol.* 15, pp. 651-670.

[20] Pang, S., Relative importance of diffusion and convective flow of moiature vapour in simulation of softwood drying, *Drying Technol.* 16, PP. 271-281, 1998.

[21] Pang, S., Langrish, T., Keey, R., The heat of sorption of timber, *Drying Technol.* 11, pp. 1071-1080, 1993.

[22] Pang, S., Langrish, T., Keey, R., Moisture movement in softwood timber at elevated temperatures, *Drying Technol.* 12, pp. 1897-1914.

[23] Simpson, W. and Rosen, H, Equilibrium moisture content of wood at high temperature, *Wood and Fiber*. 13, pp. 150-158, 1981.

[24] Simpson, W., Predicing equilibrium moisture content of wood by mathematical models, *Wood and Fibers.* 5, pp. 41-49, 1973.

[25] Skaar, C., Wood-water relations, Springer-Verlag, Berlin, 1988.

[26] Haghi, A.K., Ghanadzadeh, H., and Rondot, D.," Experimental survey on Microwave Drying of Porous Media" *Iran. J. Chem & Chem. Eng.*, Vol. 24, No. 2, 2005.

[27] Haghi, A. K., "Thermal Analysis of Drying Process- a theoretical approach, *Journal of Thermal Analysis and Calorimetry,"* Vol. 74, pp 827-840, 2003.

[28] Haghi, A. K., and Valizadeh, M., " Experimental Investigation on Microwave Drying" *International Journal of Heat and Technology*, Vol. 22, No. 2, pp167-172, 2004.

[29] Haghi,A.K.,and Ghanadzadeh,H.," A Study of Thermal Drying Process*"* *Indian Journal of Chemical Technology*, Vol. 12, 2005, pp. 654-663.

[30] Moody, L., Friction factors for pipe flow, *Trans. ASME* 66, pp. 671-684, 1994.

[31] White, F., Fluid Mechanics, third ed., McGraw-Hill, Inc., 1994.

[32] Haaland, S., Simple and explicit formulas for the friction factor in turbulent pipe flows, *J. Fluids Eng*, 1983, pp. 89-90.

[33] Dincer, I., Moisture transfer analysis during drying of slab woods, *Heat and mass Transfer*, 34, pp. 317-320, 1998.